Cancer immunoediting by melanocyte differentiation antigen-specific T cells determines response to immune checkpoint inhibition

Lukas Flatz (lukas.flatz@med.uni-tuebingen.de)
Eberhard-Karls-University Tuebingen, Germany

Sandra Ring
Kantonsspital St.Gallen

Oltin Pop
Institute of Immunobiology

Joanna Poźniak
Laboratory for Molecular Cancer Biology

Fiamma Berner
Institute of Immunobiology

Omar Ali
Institute of Immunobiology

Marie-Therese Abdou
Institute of Immunobiology

Stefan Diem
Department of Oncology and Hematology

David Bomze
The Hebrew University of Jerusalem

Rebekka Niederer
Institute of Immunobiology

Mirjam Fässler
Institute of Immunobiology

Ewout Landeloos
Laboratory for Molecular Cancer Biology

Florian Rambow
Laboratory for Molecular Cancer Biology

Greet Bervoets
Laboratory for Molecular Cancer Biology

Sandra Freiberger
Department of Pathology and Molecular Pathology

Thomas Mayr

Institute of Pathology
Michael Muders
University of Bonn
Maries van den Broek
University of Zurich https://orcid.org/0000-0002-9489-3692
Tobias Bald
QIMR Berghofer https://orcid.org/0000-0003-0061-235X
Jennifer Lansdberg
Department of Dermatology and Allergology
Dimo Dietrich
Department of Otolaryngology, Head and Neck Surgery
Joanna Mangana
Department of Dermatology
Antonio Cozzio
Department of Dermatology and Allergology
Claus Garbe
University Medical Center, Eberhard Karls University Tuebingen
Reinhard Dummer
University Hospital Zurich
Mitchell Levesque
Department of Dermatology
Wolfram Jochum
Institute of of Pathology
Burkhard Ludewig
Kantonsspital St. Gallen https://orcid.org/0000-0002-7685-573X
Oliver Bechter
Department of General Medical Oncology
Jean-Christophe Marine
Laboratory for Molecular Cancer Biology
Thomas Tüting
Laboratory for Experimental Oncology https://orcid.org/0000-0001-7146-0934
Michael Hölzel
Institute of Experimental Oncology

Article

Keywords: c,ancer immunoediting, cancer immune surveillance, tumor immunogenicity

Posted Date: May 3rd, 2021

DOI: https://doi.org/10.21203/rs.3.rs-403313/v1

Cancer immunoediting by melanocyte differentiation antigen-specific T cells determines response to immune checkpoint inhibition

Sandra S. Ring[1*], Oltin T. Pop[1]*, Joanna Poźniak[2], Fiamma Berner[1], Omar Hasan Ali[1,3], Marie-Therese Abdou[1], Stefan Diem[4,5], David Bomze[1], Rebekka Niederer[1,3], Mirjam Fässler[1], Ewout Landeloos[2], Florian Rambow[2], Greet Bervoets[2], Sandra N. Freiberger[6], Thomas Mayr[7], Michael Muders[7], Maries van den Broek[8], Tobias Bald[9], Jennifer Landsberg[10], Dimo Dietrich[11], Joanna Mangana[12], Antonio Cozzio[3], Claus Garbe[13], Reinhard Dummer[12], Mitchell P. Levesque[12], Wolfram Jochum[14], Burkhard Ludewig[1], Oliver Bechter[15], Jean-Christophe Marine[2], Thomas Tüting[16], Michael Hölzel[17], Lukas Flatz[1,3,4,12,13]

* S.S.R. and O.T.P. contributed equally to this work.

Affiliations

[1]Institute of Immunobiology, Kantonsspital St. Gallen, St. Gallen, Switzerland; [2]Laboratory for Molecular Cancer Biology, VIB Center for Cancer Biology, KU Leuven, Leuven, Belgium; [3]Department of Dermatology and Allergology, Kantonsspital St. Gallen, Switzerland; [4]Department of Oncology and Haematology, Kantonsspital St. Gallen, Switzerland; [5]Department of Oncology and Haematology, Spital Grabs, Switzerland; [6]Department of Pathology and Molecular Pathology, University and University Hospital Zurich, Switzerland; [7]Rudolf-Becker-Laboratory for Prostate Cancer Research, Institute of Pathology, University of Bonn Medical Center, Germany; [8]Institute of Experimental Immunology, University of Zurich, Zurich, Switzerland; [9]QIMR Berghofer Medical Research Institute, Brisbane, Australia; [10]Department of Dermatology and Allergy, University of Bonn, Bonn, Germany; [11]Department of Otolaryngology, Head and Neck Surgery, University Hospital Bonn, Germany; [12]Department of Dermatology, University Hospital of Zurich, University of Zurich; [13]Department of Dermatology, University Hospital of Tübingen, Germany; [14]Institute of Pathology, Kantonsspital St. Gallen, Switzerland; [15]Department of General Medical Oncology UZ Leuven, Belgium; [16]Laboratory for Experimental Dermatology, Department of Dermatology, University Hospital Magdeburg, Magdeburg, Germany; [17]Institute of Experimental Oncology, University Hospital Bonn, University of Bonn, Germany.

Corresponding author: Lukas Flatz, email: lukas.flatz@med.uni-tuebingen.de

Short title: Cancer immunoediting is associated with checkpoint inhibitor response

Abstract

T cells are critical in cancer immune surveillance but they can also shape tumor immunogenicity, described as cancer immunoediting[1,2]. Melanoma patients commonly harbor T cells recognizing melanocyte differentiation antigens (MDAs)[3-6]. However, the roles of MDA-specific T cells in shaping melanoma immunogenicity and the response to immune checkpoint inhibition remain elusive. Here, we prospectively profiled peripheral $CD8^+$ T cells from 27 stage IV patients before initiation of checkpoint inhibitor therapy. Clinical failure was associated with increased MDA-specific $CD8^+$ T cells and reduced tumor MDA expression pretreatment. In nonresponders, decreased tumor MDA expression was concomitant with a dedifferentiated melanoma phenotype. We confirmed in 30 stage III patients that individuals with relapse disease during adjuvant anti-PD-1 therapy demonstrated a significantly higher incidence of dedifferentiated tumors pretreatment than individuals without recurrence. Thus, MDA-directed $CD8^+$ T cells are associated with a dedifferentiated phenotype and reduced clinical response to checkpoint inhibitor therapy suggesting immunoediting as an important resistance mechanism.

Main

Cancer immunotherapies targeting the inhibitory checkpoint molecules PD-1 and CTLA-4 harness the patient's antitumor immunity and the presence of $CD8^+$ T cell infiltrates in tumors is generally considered a positive correlative factor for response to checkpoint inhibitor therapy[7,8]. While tumor-specific $CD8^+$ T cells play a critical role in cancer immune surveillance[9], they can also shape tumor immunogenicity to evade immune-mediated killing, a process known as cancer immunoediting[1,2]. One mechanism of cancer immunoediting was previously shown in mouse models in which adoptive transfer of $CD8^+$ T cells specific for melanosomal antigens elicited melanoma dedifferentiation in response to T cell-derived inflammatory cytokines and resulted in the loss of T cell-mediated tumor control[10-12]. However, evidence of inflammation-induced dedifferentiation[13] in humans is scarce and hitherto derived from *in vitro* human cell lines experiments[14,15], transcriptomic studies[16,17] or case reports[18]. In one patient, adoptive transfer of MART-1-specific $CD8^+$ T cells induced inflammation in the tumor microenvironment resulted in gradual loss of expression of MART-1 and other melanocytic antigens in relapsing tumors[18].

Although melanocyte differentiation antigen (MDA)-specific T cells have been studied for a long period in melanoma patients[4,19,20], surprisingly little is known about the phenotypic co-evolution between MDA-specific T cells with melanoma respectively their influence in the context of immune checkpoint inhibitor treatment.

A high proportion of melanoma patients commonly harbor $CD8^+$ T cells recognizing tumor-associated antigens such as MDAs[5,6], cancer-testis antigens (CTA)[4,21] or antigens derived from tumor-specific mutations (neo-antigens)[22] but their role in immune checkpoint therapy has not been resolved. Vitiligo is elicited by MDA-specific $CD8^+$ T cells and represents a positive correlative factor for clinical responses to immunotherapies in melanoma[23-25]. To assess MDA- and CTA-specific $CD8^+$ T cell responses in the context of checkpoint inhibitor therapy, we prospectively enrolled 27 patients with stage IV melanoma treated with an anti-PD-1 antibody

either alone or in combination with an anti-CTLA-4 antibody (St. Gallen (SG) cohort, Fig. 1a and Extended Data Table 1). All patients were treatment naïve for anti-PD-1 therapy. Consistent with published trials, 44 % of the patients in our cohort were responders, while 56% of the patients in our cohort did not show an objective clinical response at 12 weeks according to Response Evaluation Criteria in Solid Tumors (RECIST) 1.1 [26-29] (Extended Data Table 1, Extended Data Fig. 1a). To examine $CD8^+$ T cell responses, we stimulated peripheral blood mononuclear cells (PBMCs) collected before initiation of checkpoint inhibitor therapy with separate overlapping peptide pools representing the full-length sequence of the MDAs tyrosinase (TYR), MART-1, gp100 and tyrosinase-related protein 2 (TRP2) and the CTAs MAGE-A1, MAGE-A3, MAGE-A4 and NY-ESO-1 (Fig. 1b and Extended Data Fig. 1b). We found that the activity of antigen-experienced $CD45RA^{low}$ $CD8^+$ T cells was commonly directed against the MDAs TYR (21 of 27 patients), MART-1 (7 of 27 patients), and gp100 (6 of 27 patients), as indicated by the expression patterns of the cytokines IFN-γ and TNF-α (Fig. 1c, Extended Data Fig. 1c and Extended Data Fig. 2a). Fewer T cell responses were observed against the MDA TRP2 (2 of 27 patients) and the CTAs MAGE-A1 (1 of 27 patients), MAGE-A3 (1 of 27 patients), MAGE-A4 (4 of 27 patients), and NY-ESO-1 (4 of 27 patients) (Extended Data Fig. 1c to e). Therefore, within this study we further focused on $CD8^+$ T cells specific for the MDAs TYR, MART-1, and gp100. Interestingly, substantially higher proportions of nonresponders (NRs) than responders (Rs) showed increased IFN-γ^+ and TNF-α^+ $CD8^+$ T cell responses against TYR, MART-1 and gp100 (Fig. 1c and d, Extended Data Fig. 1c and d and Extended Data Fig. 2a and b). Moreover, the nonresponders were characterized by a broader MDA-specific $CD8^+$ T cell response, defined as cytokine-expressing $CD8^+$ T cells against any of the melanocytic antigens TYR, MART-1 or gp100 (Fig. 1c and e and Extended Data Figure 2a and c). Likewise, the frequency of cytokine-producing $CD8^+$ T cells specific for the three MDAs combined was significantly higher in the nonresponders compared to responders (Fig. 1c and f and Extended Data Fig. 2a and d). In sum, our data show that

98 nonresponders exhibit a higher proportion of MDA-specific $CD8^+$ T cells prior to checkpoint
99 inhibitor therapy.
100 A T cell-mediated immunoselection process can result in the outgrowth of tumor cells lacking
101 expression of immunodominant antigens[30]. To investigate the relationship between MDA-specific
102 T cells and MDA tissue expression, we performed quantitative immunohistochemical (IHC)
103 analysis for TYR, MART-1 and gp100 of pretreatment tumor samples from 19 patients in the SG
104 cohort (R=10, NR=9; Fig. 2a and b). The percentage of tumor cells expressing each of these
105 antigens was assessed as outlined in Extended Data Figure 3. Tumor cells of responders showed a
106 higher frequency of expression of the individual MDAs TYR, MART-1 and gp100 compared to
107 nonresponders (Fig. 2c and d). Moreover, expression levels of individual MDAs were not only
108 decreased in nonresponders but we observed a broad loss of all melanocytic proteins in
109 nonresponders (7 of 9 nonresponder, patients 1, 8, 14, 18, 19, 20 and 21) compared to responders
110 (9 of 10 responders, patients 2, 4, 5, 11, 12, 15, 17, 22, 25) as described by the reduced breath of
111 the expression of TYR, MART-1 and gp100 combined (Fig. 2c). Finally, Spearman's correlation
112 analysis revealed an inverse correlation between tumor MDA expression in pretreatment biopsies
113 and MDA-specific $CD8^+$ T cell responses in blood (Fig. 2c and e, Spearman $r = -0.5666$, $P = 0.01$).
114 These observations showed that the broad loss of melanocytic antigen expression together with
115 increased MDA-specific $CD8^+$ T cells in the periphery are associated with an impaired response
116 to checkpoint inhibitor therapy. Thus, MDA-directed T cell responses may have an
117 underappreciated yet crucial role in shaping melanoma immunogenicity and affecting the clinical
118 outcome to immune checkpoint inhibitors.
119 A critical role of T cell responses against MDAs in melanoma emanates from therapies using
120 adoptive transfer of either *ex vivo* expanded tumor-infiltrating lymphocytes or TCR-engineered
121 T cells recognizing MDAs[31,32]. In mouse melanoma models, adoptive transfer of T cells targeting
122 a melanosomal antigen compared to transfer of T cells against an oncogenic antigen, provoked

123 profound dedifferentiation[11]. Therefore, dedifferentiation represents an important evasion
124 mechanism in response to T cell-mediated immune pressure[12,13]. In our study, we have observed
125 high pre-existing MDA-specific $CD8^+$ T cells concomitant with a broad loss of melanocytic
126 antigen expression predominantly in nonresponders. Next, we investigated whether tumors with
127 reduced MDA tissue antigen levels also exhibited a dedifferentiated phenotype rather than only
128 selective downregulation of melanocytic antigens. Melanoma dedifferentiation proceeds along a
129 differentiation trajectory that can be subclassified into four subtypes ranging from melanocytic
130 and transitory to neural crest-like and undifferentiated[16,33]. To assess whether progression along
131 the dedifferentiation trajectory described by Tsoi et al. in melanoma cell lines[33] can be discerned
132 in patient samples, we performed single-cell RNA sequencing (scRNA-seq) of melanoma
133 metastases collected from 15 stage III or stage IV patients (Cohort Leuven; Extended Data Table
134 2; 14 of the 15 patients were drug-naive). Unsupervised clustering of all 15 tumor lesions
135 combined using Harmony integration and Uniform Manifold Approximation and Projection
136 (UMAP) revealed 11 distinct clusters (Fig. 3a and Extended Data Fig. 4a and b). We leveraged the
137 gene signatures for the melanoma differentiation subtypes identified by recent transcriptomic
138 analysis[33,34] and created corresponding scores for each subtype (Extended Data Tables 4 and 5).
139 Based on these scores, we detected different melanoma differentiation cell states in this patient
140 cohort. Tumor cells in clusters 1, 4, 5, 6, 8 and 10 showed a melanocytic (i.e., differentiated)
141 phenotype with a high pigmentation signature, while tumor cells in clusters 0, 2 and 3 and 7 were
142 in a transitory state with reduced pigmentation levels (Fig. 3b and Extended Data Fig. 4c and d).
143 In contrast, melanoma cells in clusters 2, 3, 7 and 9 were identified as dedifferentiated phenotype
144 as characterized by increased expression of genes associated with a neural crest-like cell signature
145 (cluster 2, 7 and 9) or a an undifferentiated (i.e., “invasive”) phenotype (cluster 3 and 9) (Fig. 3b).
146 Likewise, cells in clusters 2, 3, 7 and 9 demonstrated a reduced pigmentation signature as well as
147 MDA expression and increased expression levels of neural crest stem cell (NCSC) and epithelial-

mesenchymal transition (EMT) markers (Extended Data Fig. 4c and d). In addition, levels of the transcription factor *MITF,* the master regulator of melanocytic differentiation[35,36], were decreased in melanoma cells in clusters 2, 3 and 9 (Fig. 3c), all of which harbor the dedifferentiated melanoma phenotype (Fig. 3b). Moreover, we observed increased expression of the receptor tyrosine kinase *EGFR* in clusters 3 and 9, while tumor cells from clusters 2 and 7 expressed the neural crest marker *NGFR* (Fig. 3c), both marker are linked to a dedifferentiated melanoma phenotype[10,14,37,38]. Overall, this single-cell transcriptomic analysis in treatment-naïve clinical samples established the presence of melanoma cells exhibiting distinct differentiation statuses ranging from cells with either a melanocytic differentiated phenotype to a dedifferentiated phenotype with reduced melanocytic antigen expression.

Next, we sought to investigate whether tumor cells from patients in the SG cohort not only exhibited reduced expression of melanocytic antigens but show a dedifferentiated phenotype. We performed quantitative IHC analysis of the 19 available biopsies obtained prior to treatment (Fig. 3d-g, Fig 2a, Extended Data Fig 3) and examined tissue expression of MITF, EGFR and NGFR, markers associated with dedifferentiated tumors according to our scRNA-seq data (Fig. 3). Strikingly, our IHC analysis revealed significantly reduced expression of MITF and markedly increased frequency of tumor cells expressing EGFR in nonresponders compared to responders, whereas the expression of NGFR was not different (Fig. 3d and e, Extended Data Fig. 5a to c). We further defined tumor cells with low MITF expression ($MITF^{low}$) and high EGFR expression ($EGFR^{high}$) as dedifferentiated melanomas based on threshold values determined for each protein by receiver operator characteristic (ROC) curves (Fig. 3e, green boxes). Dedifferentiated $MITF^{low}$ $EGFR^{high}$ tumors were identified exclusively in nonresponders (8 out of 9), while tumors from responders showed a uniformly differentiated and melanocytic phenotype (Fig. 3e and Fig 2c and and f, Extended Data Figure 5d and e). Moreover, compared to patients with differentiated tumors, patients with dedifferentiated tumors demonstrated significantly diminished progression-free

173 survival (Fig. 3g). Thus, melanoma patients with reduced MDA expression not only selectively
174 downregulated these antigens but rather exhibited a dedifferentiated phenotype which was
175 exclusively found in nonresponders.
176 Finally, to strengthen our findings that patients with dedifferentiated melanomas are associated
177 with poor outcome to checkpoint inhibitor treatment, we obtained tumor biopsies from 30 stage
178 III melanoma patients before initiation of adjuvant checkpoint inhibitor therapy (Zurich (ZH)
179 cohort, Extended Data Table 3). Adjuvant anti-PD-1 therapy after surgical resection of regional
180 lymph node metastases has become the standard of care in melanoma patients, resulting in
181 significantly longer recurrence-free survival than placebo treatment[39,40]. In this independent
182 cohort, 37% of patients developed recurrence within the observed time (Relapses; Rel), whereas
183 63% remained disease-free (Disease-Free; DF) (Fig. 4a, Extended Data Fig. 6a). We performed
184 IHC analysis of the collected biopsies and quantified the expression of MITF, EGFR, NGFR (Fig.
185 4b and c and Extended Data Fig. 6b to d). In this validation cohort, 47% of patients (14 out of 30)
186 presented with a $MITF^{low}$ $EGFR^{high}$ and/ or $MITF^{low}$ $NGFR^{high}$ dedifferentiated tumor phenotype.
187 Strikingly, individuals with relapsed disease were characterized by a significantly higher incidence
188 of dedifferentiated tumors than patients without recurrence (Fig. 4c and d, Extended Data Figure
189 6b to f). Accordingly, adjuvant anti-PD-1 treated patients with a dedifferentiated tumor phenotype
190 exhibited significantly shorter progression-free survival than those with a differentiated tumor
191 phenotype (Fig. 4e). Together, these data demonstrate that patients with a dedifferentiated
192 melanoma prior to treatment initiation are associated with therapeutic resistance to adjuvant
193 immune checkpoint therapy. Importantly, we have shown that dedifferentiated melanomas impacts
194 therapy response independent of the stage of the tumor.
195 In this study, immune profiling of peripheral T cells revealed an interrelationship among MDA-
196 directed $CD8^+$ T cell responses and reduced expression of the MDAs TYR, MART-1 and gp100
197 in the tumor tissue. Additionally, MDA downregulation was correlated with an increased incidence

198 of a dedifferentiated phenotype and poor clinical outcome following immune checkpoint
199 inhibition. Taken together, we showed in two independent cohorts of patients with different tumor
200 stages (stages III and IV) that a differentiated phenotype is negatively associated with the response
201 to immune checkpoint inhibitor blockade.
202 Increased T cell infiltrates into tumors[7,8] as well as T cell-mediated adverse events, such as vitiligo
203 which is elicited by MDA-specific $CD8^+$ T cells[23-25], represent a positive correlation with clinical
204 outcome. However, these tumor-specific immune responses can, at the same time, promote cancer
205 immunoediting and affect clinical response to treatment. During the course of disease, cancer
206 immunoediting by MDA-specific $CD8^+$ T cells may drive the evolution of tumor cells resulting in
207 reduced MDA expression and, ultimately, the loss of melanocytic identity. Tumors in patients may
208 fall into one of the three phases of the immunoediting process - elimination, equilibrium or escape[2]
209 - and can result in different clinical outcomes to checkpoint inhibitor treatment.
210 Immune checkpoint blockade with anti-PD-1 re-invigorates pre-existing tumor-specific $CD8^+$ T
211 cells in a large proportion of melanoma patients but only 40 % of the patients respond clinically[41].
212 Thus, based on our data, we hypothesize that release of $CD8^+$ T cells targeting melanocytic
213 antigens upon PD-1 therapy results in immune-mediated elimination of melanoma cells in patients
214 with differentiated tumor phenotypes. In contrast, releasing the brakes on pre-existing MDA-
215 specific $CD8^+$ T cells in patients with dedifferentiated tumors may be less effective because (i)
216 these tumors have lost their melanocytic identity and thus the expression of melanocytic antigens
217 during the course of disease and (ii) MDA-specific $CD8^+$ T cells may outcompete the expansion
218 of T cells with other specificities. Kvistborg et al. have studied $CD8^+$ T cell responses to
219 melanoma-associated epitopes in patients receiving anti-CTLA-4 therapy using HLA-*0201-
220 restricted tetramers. Within their study, they have identified pre-existing melanoma-specific T cell
221 prior to treatment but did not relate them to therapeutic outcome to immune checkpoint blockade[19].
222 In our study, we have employed an HLA-independent methodological approach using overlapping

peptide pools which unveiled a high level of detectable MDA- and to a lesser extent CTA-specific $CD8^+$ T cells prior to checkpoint inhibitor treatment and markedly increased frequencies of the MDAs TYR, MART-1 and gp100 were detected in nonresponders compared to responders. Therefore, our study suggests that MDA-directed T cells have a more profound impact on different melanoma therapies than currently assumed. Understanding the co-evolution of melanoma cells in response to immunological pressure by T cells targeting melanocytic antigens is critical to improve the outcome of patients treated with cancer immunotherapies and in the design of new treatments targeting dedifferentiated tumors.

Our study is not without caveats. First, it characterizes $CD8^+$ T cell responses against a limited number of melanoma-associated antigens without considering $CD8^+$ or $CD4^+$ T cell responses specific for other antigens. Second, our study cohorts are relatively small. Still, we have validated and combined our findings in three independent patient cohorts and these findings are based on strong data generated in mouse models[10,11,16]. Third, in almost all patients we only analyzed one available tumor lesion obtained at a time point close to initiation of checkpoint inhibitor therapy and the collection of PBMCs. However, further studies should evaluate the tumor phenotype and the corresponding T cell responses during the time course of the disease as well as in multiple lesions. Lastly, we suggest that immune-mediated dedifferentiation is an important resistance mechanism for immune checkpoint inhibitor therapy in melanoma; yet this resistance mechanism may be transferable to other tumor entities.

Main Figures

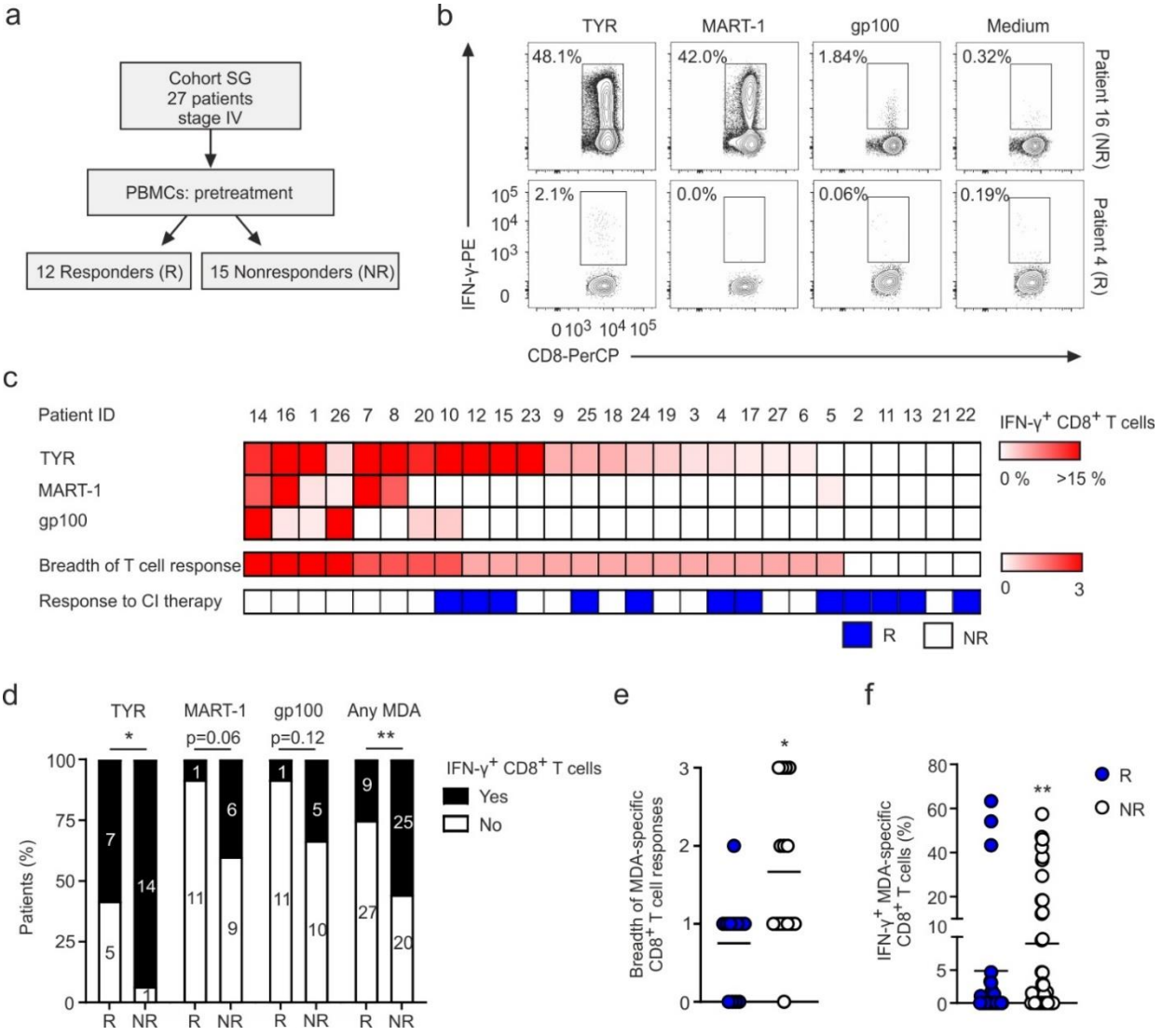

Figure 1. Levels of pre-existing MDA-specific CD8⁺ T cells in melanoma patients receiving checkpoint inhibitor therapy. a, In the prospective St.Gallen (SG) cohort, peripheral blood mononuclear cells (PBMCs) were obtained from 27 patients with stage IV melanoma prior to checkpoint inhibitor therapy. Clinical responders (R; N=12) and nonresponders (NR; N=15) were determined at 12 weeks. **b-f,** CD8⁺ T cell responses against the melanocyte differentiation antigens (MDAs) TYR, MART-1 and gp100 after *in vitro* stimulations of PBMCs with overlapping 15-mer peptide pools for each individual antigen for 10 days as measured by IFN-γ expression. **b,** Representative FACS plots of samples from patient 16 (NR) and patient 4 (R). **c,** Heatmaps summarizing the frequency of IFN-γ-producing CD8⁺ T cells for the indicated antigens. The color scale represents the frequency of IFN-γ⁺ CD3⁺ CD8⁺ CD45RA^{low} T cells. The breadth of the CD8⁺ T cell response was defined as the number of the individual IFN-γ⁺ CD8⁺ T cells against the MDAs TYR, MART-1 and gp100, as indicated by the detection of IFN-γ⁺ CD8⁺ T cell responses, ranging from 0 (none) to 3 (all). **d,** Proportions of R and NR with MDA-specific CD8⁺ T cell responses to the individual MDAs or any MDA. **e,** Summary of the breadth of MDA-specific CD8⁺ T cells in R and NR as shown for individual patients as shown in panel c. **f,** Frequencies of IFN-γ⁺ CD8⁺ T cells against any MDA (TYR, MART-1 or gp100) in R vs NR. Dots represent individual patients, and lines indicate the mean values (e and f). Statistical analysis was performed using the chi-square test (d) and Mann-Whitney test (e and f); *P < 0.05, **P < 0.01, ***P < 0.001.

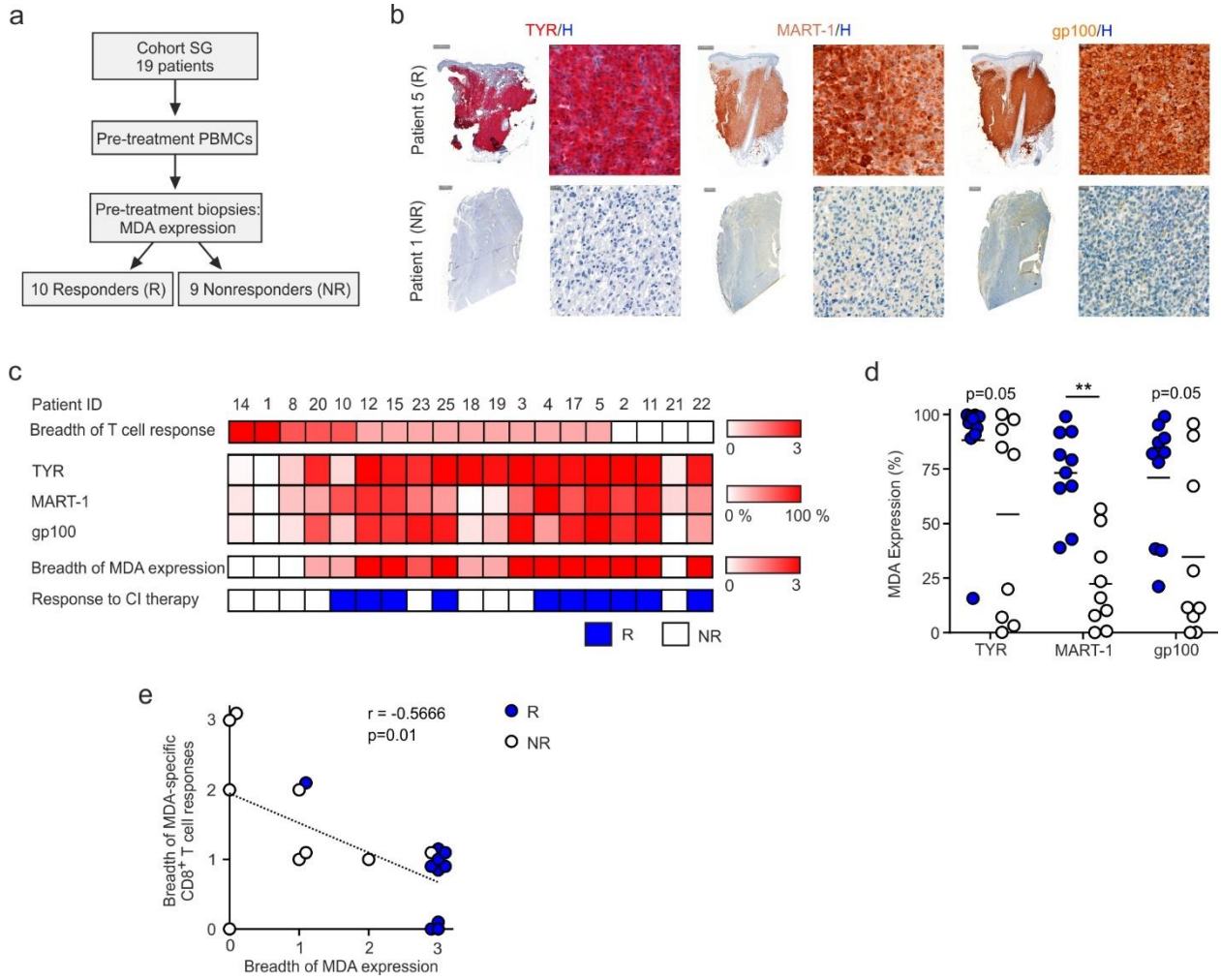

Figure 2. MDA tissue expression inversely correlates with peripheral MDA-specific CD8⁺ T cells. a, In 19 of the patient from the SG cohort, tumor biopsies obtained before initiation of checkpoint inhibitor therapy and matched PBMCs from Fig. 1 were analyzed. The expression of the MDAs TYR, MART-1 and gp100 was analyzed using quantitative IHC analysis of biopsy tissue. **b,** Representative images for the indicated antigens in patient 5 (R) and patient 1 (NR). The frequency of tumor cells expressing each of these antigens was assessed as outlined in Extended Data Figure 3. Hematoxylin (H) staining to identify the cell nucleus. Scale bars are 500 and 2000 µm for the general images (top and bottom images) and 20 µm for the magnified images. **c,** Heatmaps summarizing the frequency of melanoma cells stained positive for the MDAs TYR, MART-1 and gp100. The breadth of MDA expression was defined as the number of MDAs expressed per patient sample ranging from 0 (none) to 3 (all) as defined by values from ROC curves for each individual antigen. The breadth of T cell response (data from Fig. 1) is specified as the number of individual MDAs recognized, as indicated by the detection of IFN-γ⁺ CD8⁺ T cell responses, ranging from 0 (none) to 3 (all). **d,** Frequencies of melanoma cells showing positive staining for each of the MDAs TYR, MART-1 and gp100 in the analyzed tissue slides between R and NR. Dots represent individual patients, and lines indicate mean values. **e,** Correlation between the breadth of MDA expression and that of MDA-specific CD8⁺ T cell responses. Dots represent individual patients. Statistical analysis was performed using the Mann-Whitney test (d) and Spearman's correlation (e); *P < 0.05, **P < 0.01, ***P < 0.001.

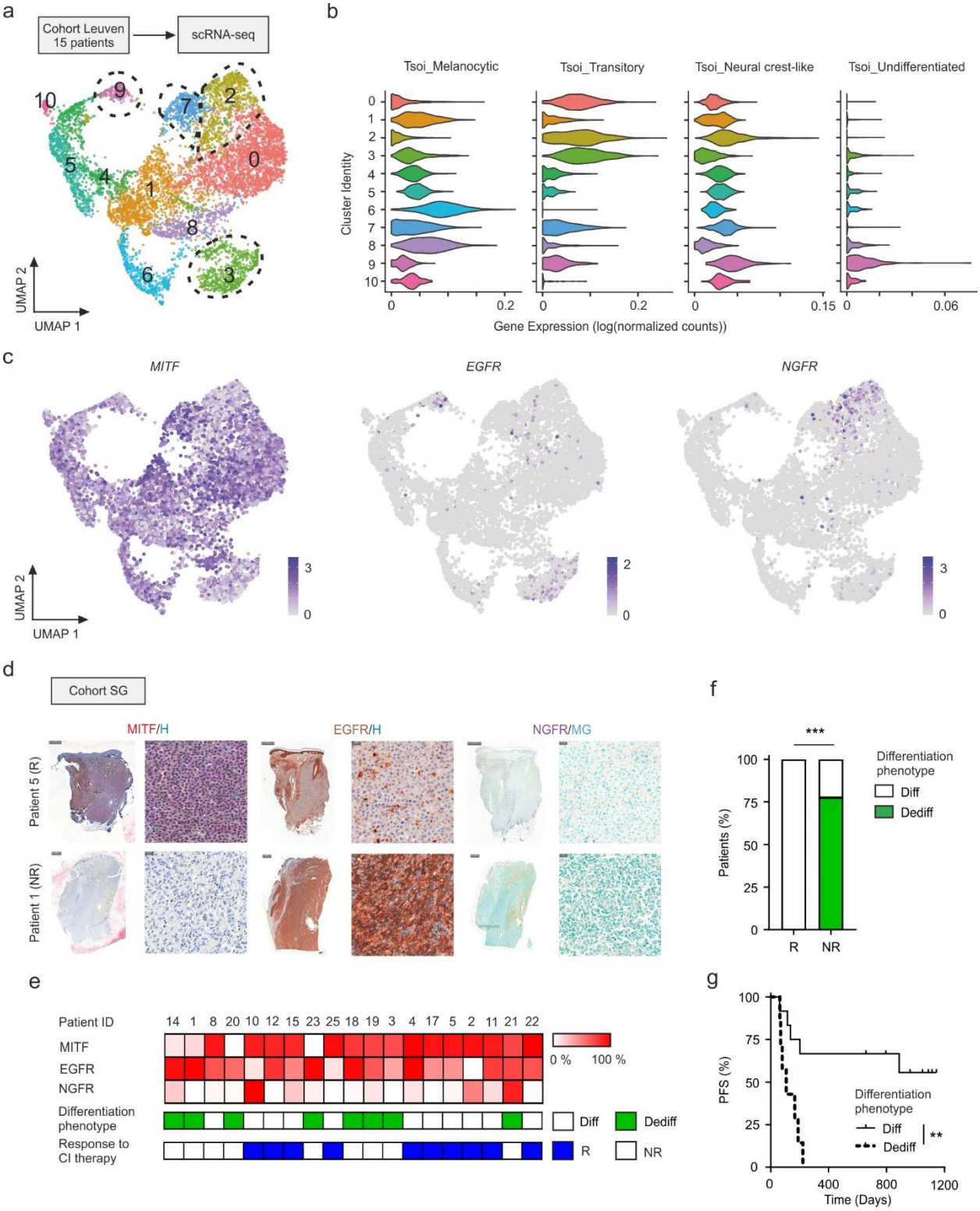

Figure 3. The dedifferentiated melanoma phenotype predicts patient outcome in response to checkpoint inhibitor therapy. a-c, We collected melanoma metastases from 15 stage III or stage IV treatment-naïve patients and performed single-cell RNA-seq analysis of tumor cells (Leuven cohort). **a**, UMAP plot displaying cluster assignment. Highlighted clusters harbor tumor cells with a dedifferentiated phenotype (cluster 2, 3, 7 and 9) whereas the other cluster exhibit a melanocytic and differentiated phenotype. **b**, Violin plots based on the Tsoi et el. (2018) gene signatures for melanocytic, transitory, neural crest-like and undifferentiated melanoma phenotypes. **c**, UMAP plots showing the gene expression of

MITF, *EGFR* and *NGFR*. **d-g**, In the SG cohort, the expression of MITF, EGFR and NGFR was assessed in tumor biopsies obtained before initiation of checkpoint inhibitor therapy by quantitative IHC analysis. **d**, Representative images for the indicated antigens in patient 5 (R) and patient 1 (NR). The frequency of tumor cells expressing each of these antigens was assessed as outlined in Extended Data Figure 3. Hematoxylin (H) or Methyl Green (MG) staining to identify the cell nucleus. Scale bars are 500 and 2000 µm for the general images (top and bottom images) and 20 µm for the magnified images. **e,** Heatmaps summarizing the frequencies of melanoma cells showing positive staining for MITF, EGFR or NGFR using quantitative IHC analysis. The dedifferentiated melanoma phenotype (Dediff) was defined as $MITF^{low}$ $EGFR^{high}$ or $MITF^{low}$ $NGFR^{high}$ as based on threshold values from ROC curves for each individual protein. **f,** Proportions of patients in the 19 patients from the SG cohort with a dedifferentiated phenotype in the R and NR groups. **g,** Progression-free survival of patients with a dedifferentiated or differentiated melanoma phenotype. Statistical analysis was performed using the chi-square test (f) or the Mantel-Cox log-rank test (g); *P < 0.05, **P < 0.01, ***P < 0.001.

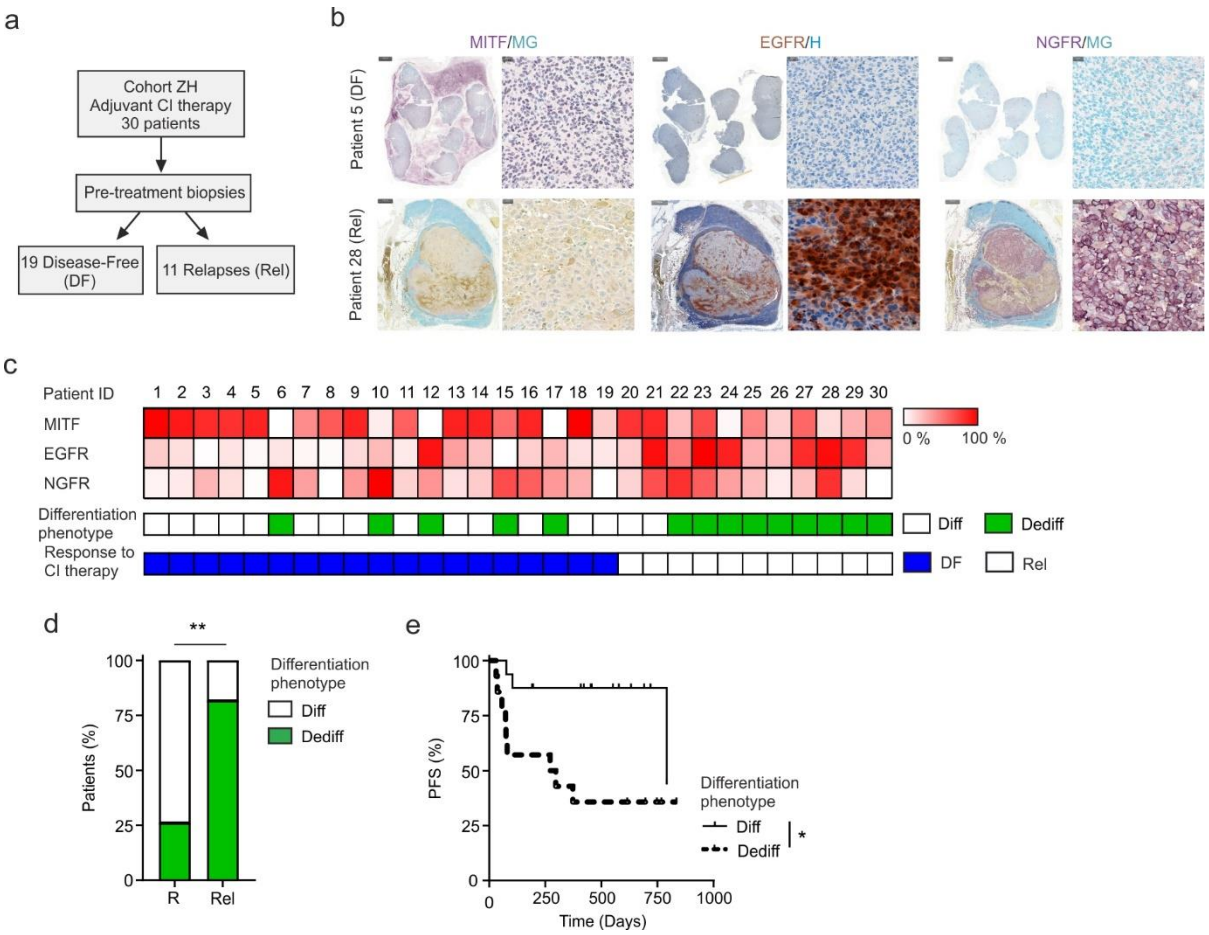

Figure 4. The dedifferentiated melanoma phenotype predicts patient outcome in response to adjuvant anti-PD-1 therapy. a, In the Zurich (ZH) adjuvant cohort, tumor biopsies were obtained before initiation of adjuvant anti-PD-1 treatment. Disease-Free patients (DF; R; n=19) and patients who experienced relapse (Rel; n=11) were determined at the first PET-CT scan within 3 months after start of therapy. **b,** Representative images showing the expression of MITF, EGFR and NGFR in patient 5 (DF) and patient 28 (Rel). The frequency of tumor cells expressing each of these antigens was assessed as outlined in Extended Data Figure 3. Hematoxylin (H) or Methyl Green (MG) staining to identify the cell nucleus. Scale bars are 1000 and 2000 µm for the general images (top and bottom images) and 20 µm for the magnified images. **c,** Heatmaps summarizing the frequency of tumor cells stained positive for MITF, EGFR and NGFR using quantitative IHC analysis. The dedifferentiated phenotype (Dediff) was defined as $MITF^{low}$ $EGFR^{high}$ or $MITF^{low}$ $NGFR^{high}$ and based on threshold values from ROC curves for each individual protein. **d,** Proportions of patients in the ZH adjuvant anti-PD-1 cohort with a dedifferentiated phenotype in the DF and Rel groups. **e,** Progression-free survival of patients with a dedifferentiated or differentiated melanoma phenotype. Statistical analysis was performed using the chi-square test (d) or Mantel-Cox log-rank test (e); *P < 0.05, **P < 0.01, ***P < 0.001.

Material and Methods

Ethical Approval

All patients provided written informed consent. All study procedures were performed in accordance with the principles of the Declaration of Helsinki and applicable Swiss and Belgian laws and regulations, and approved by the Ethics Committee of Eastern Switzerland (BASEC Nr. 2016-00998, BASEC Nr. PB_2017-00494) and UZ Leuven Medical Ethical Committee (S62275).

Patients

In this prospective study, 27 patients with unresectable stage IV melanoma at Kantonsspital St. Gallen were included (SG cohort, see Extended Data Table 1 for patient information). Patients were treated with antibodies against the checkpoint inhibitor molecules PD-1 (pembrolizumab or nivolumab) either alone or in combination with anti-CTLA-4 (ipilimumab) and were included only if they had not received prior anti-PD-1 treatment. Tumor responses were evaluated by CT imaging after 8-12 weeks using RECIST 1.1[27]. According to these criteria, patients who achieved complete remission (CR) or partial remission (PR) were categorized as clinical responders (Rs), and those with stable disease (SD) or progressive disease (PD) were categorized as clinical nonresponders (NRs). For each patient, blood was drawn before start of immune checkpoint therapy. PBMCs were isolated using Ficoll-Paque gradient centrifugation and cryopreserved at -150°C. In addition, available pretreatment formalin-fixed and paraffin-embeded metastatic lesion biopsies taken for routine histopathological diagnosis from 19 patients in the SG cohort (10 Rs; 9 NRs) in proximity to the therapy start were used for IHC analysis.

In the second cohort, the Leuven cohort, metastatic lesion biopsies from 15 patients with locally advanced or metastatic melanoma (stage IIIB to stage IV) were collected as part of the noninterventional prospective study SPECIAL (prospective serial biopsy collection before and during immune checkpoint inhibitor therapy in patients with malignant melanoma) and used for

single-cell RNA sequencing. Almost all patients (N=14) were treatment naïve. Details of the samples are summarized in Extended Data Table 2.

A validation cohort of 30 stage III melanoma patients at the University Hospital Zurich who received anti-PD-1 (pembrolizumab or nivolumab) as adjuvant therapy was used to confirm our findings (ZH cohort, see Extended Data Table 3 for patient information). Response to therapy was assessed at the first PET-CT scan (within 3 months after start of therapy) using RECIST 1.1 criteria[27], and patients were classified as either disease-free (DF) or experiencing a relapse (Rel) during the observation (up to 1 year after treatment cessation). Available pretreatment formalin-fixed and paraffin-embedded tumor biopsies taken for routine histopathological diagnosis from all the patients in proximity to the therapy start were used for IHC analysis (19 DF; 11 Rel).

T cell stimulation assays and flow cytometry

For each patient, blood was drawn before the start of therapy, and PBMCs were isolated using Ficoll-Paque density gradient centrifugation and cryopreserved at -150° C. To assess T cell responses, PBMCs were thawed and cultured at 37°C and 5% CO_2 in RPMI 1640 medium containing 8% human serum (Biowest, catalog number S4190-100), 1% penicillin-streptomycin, 1% L-glutamine, 1% nonessential amino acids, 1% sodium pyruvate, 0.1 mg/mL kanamycin and 0.1% β-mercaptoethanol. PBMCs were seeded in 24-well plates at a density of 0.5-1x10^6 cells per well and stimulated with 15-mer peptide pools (2 μg/mL peptide) with an 11-amino-acid overlap for the following MDAs and CTAs according to the manufacturer's instructions: gp100, TYR, TRP-2, MART-1, MAGE-A1, MAGE-A3, MAGE-A4, and NY-ESO-1 (JPT, Melanoma PepMix). Every second day, half of the culture medium was replaced with fresh medium supplemented with 15000 IU/mL recombinant human IL-2 (ProLeukin, Roche). After 10 days, the cells were washed and restimulated for 6 hours with 2 μg/mL cognate peptide pools in the presence of 10 μg/mL brefeldin-A (Sigma), followed by staining for flow cytometry. PBMCs were stained with Aqua (BV510, BD, dilution 1:1000) according to the manufacturer's instructions to exclude dead cells

and with antibodies against CD8 (PerCP, clone SK1, dilution 1:100), CD3 (APC-Cy7, clone OKT3, dilution 1:100), CD45RA (BV711, clone HI100, dilution 1:400), CD4 (PE/Cy, clone OTK4, dilution 1:100) in FACS buffer (1xPBS, 2% FCS, 5 mM EDTA, 0.1% Sodium azide) for 20 min at 4°C. For intracellular staining, cells were fixed and permeabilized using the BD Cytofix/Cytoperm (BD Biosciences) and staining with TNF-α (APC, clone Mab11b, dilution 1:100) and IFN-γ (PE, clone B27, dilution 1:100) was done in permeabilization buffer (1xPBS, 2% FCS, 5 mM EDTA, 0.1% Saponin, 0.1% Sodium azide) for 40-60 min at 4°C. Samples were run on an LSR Fortessa, and flow cytometry data were analyzed with FlowJo software (TreeStar). Antigen-specific $CD8^+$ T cell responses were identified by subtracting the frequency of IFN-γ^+ and TNF-α^+ $CD8^+$ T cells from the unstimulated control and using a cutoff value of 1% IFN-γ^+ or TNF-α^+ cells.

Immunohistochemistry

Available baseline tissue samples taken for diagnostic histological examination were fixed in formalin and embedded in paraffin in the Pathology Department of KSSG using standard processing protocols. Four-micron-thick serial sections were cut using a Leica RM2255 rotary microtome (Leica Microsystems, CH). Single-epitope enzymatic immunohistochemistry on FFPE tissues was performed on serial sections to assess the expression of TYR, MART-1, gp100, MITF, EGFR, and NGFR within the tumors (immunohistochemical protocols for each antigen are described in the subsequent sections). Morphometric analysis was carried out on whole-slide scans acquired with a Panoramic 250 Flash III digital slide scanner (3D Histech, CH). Quantitative morphometry was performed using the QuPath v0.1.2 software platform for whole-slide image analysis (Edinburgh, UK)[42] in order to determine the percentage of tumor cells expressing the antigens interrogated by immunohistochemistry.

Tyrosinase and MITF enzymatic immunohistochemistry

FFPE tissues were sliced at a thickness of 4 µm using a rotary microtome and placed on poly-L-lysine-coated slides. The slides were dewaxed in xylene, rehydrated, subjected to heat-induced epitope retrieval (HIER) in a microwave oven using a pH 9 target retrieval solution (catalog number S2367, Dako, DK) for TYR and a pH 6 target retrieval solution (catalog number S1699, Dako, DK) for 40 minutes, and allowed to cool to room temperature. Endogenous alkaline phosphatase activity was blocked using the dual endogenous blocking solution from the EnVisionTM G/2 Doublestain System, Rabbit/Mouse (DAB+/Permanent Red) (catalog number K536111-2, Dako, DK) for 10 minutes at room temperature, followed by an avidin/biotin blocking step for 30 minutes at room temperature (catalog number SP-2001, Vector Laboratories, CA, USA), a 30-minute incubation with 3% skim milk at room temperature, and an overnight incubation at 4°C with a mouse monoclonal anti-human TYR primary antibody (catalog number M3623, Dako, DK; dilution 1:50) and mouse monoclonal anti-human MITF primary antibody (catalog number M3621, Dako, DK; dilution 1:25). The next day, the slides were incubated for 1 hour at room temperature with a biotinylated anti-mouse secondary antibody (catalog number 115-065-062, Jackson ImmunoResearch, Cambridge, UK; dilution 1:500), followed by another 1-hour incubation at room temperature with a streptavidin-AP conjugate (ref. 434322, Invitrogen, IL, USA; dilution 1:100). The signal was visualized using the Warp Red chromogen kit (catalog number WR 806, Biocare Medical, CA, USA). The slides were dehydrated with alcohol, cleared with xylene and mounted with Pertex (catalog number 41-4011-00, Medite, DE) after hematoxylin counterstaining (catalog number 8947.1, Roth, DE).

MART-1, gp100, and EGFR enzymatic immunohistochemistry

Single-epitope enzymatic immunohistochemistry for MART-1, gp100, and EGFR in FFPE tissues was performed on serial sections using a Leica BOND MAX III automated immunostainer (Leica, CH) and the following antibodies according to the manufacturer's instructions: monoclonal mouse

anti-human Melan A (Dako, catalog number M7196, clone A103, dilution 1:150, HIER - pH 9/20 minutes/95°C, incubation for 15 min), monoclonal mouse anti-human Melanosome (gp100) (Dako, catalog number M0634, clone HMB-45, dilution 1:100, HIER - pH 6/20 minutes/100°C, incubation for 30 minutes), and monoclonal mouse anti-human EGFR (Leica Biosystems, catalog number NCL-EGFR-384, dilution 1:60, HIER - pH 9/30 minutes/95°C, incubation for 60 minutes). The signal was visualized using the Leica Bond Polymer Refine Detection Kit (catalog number DS9800, Leica Biosystems, CH) and the AEC chromogen (catalog number K050-110, Diagnostic BioSystems, CH).

NGFR enzymatic immunohistochemistry

FFPE tissues were sliced at a thickness of 4 µm using a rotary microtome and placed on poly-L-lysine-coated slides. The slides were dewaxed in xylene, rehydrated, subjected to HIER using a pH 9 target retrieval solution (catalog number S2367, Dako, DK) for 20 minutes in a microwave oven, and allowed to cool to room temperature. Endogenous horseradish peroxidase activity was blocked by a 10-minute incubation at room temperature with 3% hydrogen peroxide solution (catalog number 160-0-029, Laboratorium Dr. G. Bichsel AG, CH), followed by an avidin/biotin blocking step (catalog number SP-2001, Vector Laboratories, CA, USA) for 30 minutes at room temperature, a 30-minute incubation with 3% skim milk at room temperature, and an overnight incubation at 4°C with a rabbit monoclonal anti-human p75 NGF receptor primary antibody (catalog number ab221212, Abcam, USA; dilution 1:100). The next day slides were incubated for 30 minutes at room temperature with an anti-rabbit biotinylated secondary antibody (catalog number D30-1, GBI Labs, Bothell, WA, USA; dilution 1:200), followed by another 30-minute incubation at room temperature with HRP-conjugated streptavidin (catalog number D30-1, GBI Labs, Bothell, WA, USA; dilution 1:200). The signal was visualized using a Vector VIP peroxidase substrate kit (catalog number SK-4600, Vector Laboratories, CA, USA). The slides were dehydrated with alcohol, cleared with xylene and mounted with Pertex (catalog number 41-

4011-00, Medite, DE) after methyl green counterstaining (catalog number H-3402, Vector Laboratories, CA, USA).

Image analysis

Quantitative morphometry was performed on all stained slides using the QuPath v0.1.2 software platform for whole-slide image analysis (Edinburgh, UK)[42]. Whole-slide scans acquired with a Panoramic 250 Flash III digital slide scanner (3D Histech, CH) were individually loaded into the software. For each staining vector (i.e., color), estimates of the background staining were applied to maximize differences in expression in QuPath by selecting a region of interest containing an area of background along with examples of strong nuclear counterstaining and chromogen staining and applying QuPath's "Estimate stain vectors" command to identify stain vectors within this region. The "Cell detection" command was then used to identify cells across the entire tissue section based upon nuclear identification. The full extent of each cell (area occupied by the cell) was estimated based upon measurements of intensity and morphology, including nuclear area, circularity, staining intensity for counterstaining and chromogen staining, and nucleus/cell area ratio. A two-way boosted decision tree classifier was then interactively trained to distinguish tumor cells from all other detected artefacts (comprising nontumor epithelial cells, immune cells, stromal cells, necrosis, and any artefacts misidentified as cells). Cells were classified as positive or negative based upon a single-intensity threshold applied to the maximum optical density of the detected chromogen within the nucleus or cytoplasm of the cell depending on the expression pattern (the threshold was adjusted for a random region of interest containing both negative and highly positive tumor cells until all the cells defined as positive by the software matched those considered positive by the evaluator). Summary scores were generated as the percentage of cells classified as positive after "other" detections were removed.

Library construction and sequencing

Metastatic lesions of 15 patients with locally advanced or metastatic melanoma (stage IIIB to stage IV, 14 treatment-naive) were collected and scRNA-seq analysis was performed. Libraries for scRNA-seq were created using the 10X Genomics Chromium platform according to the manufacturer's instructions. Library construction was performed with the Chromium Single Cell 3′ GEM, Library & Gel Bead Kit v3 (n = 16; 10x Genomics, catalog number 1000092) or the Chromium Single Cell A Chip Kit and 5′ Library & Gel Bead Kit (10x Genomics, catalog number 1000014). We opted for high target recovery (median 5000, range 5000-10000), keeping within the range of optimal input concentration per target recovery, as recommended by the manufacturer. In brief, cells were partitioned into gel bead-in-emulsions (GEMs) at limiting dilutions, where lysis and reverse transcription occurred, yielding uniquely barcoded full-length cDNA from polyadenylated mRNA. GEMs were subsequently broken, and the pooled fraction was amplified and subjected to fragmentation, end repair and adaptor ligation of size-selected fractions.

scRNA-seq data acquisition and preprocessing

All libraries were sequenced on an Illumina NextSeq, HiSeq4000 or NovaSeq6000 until sufficient saturation was reached (73.8% on average). After quality control, the raw sequencing reads were aligned to the human reference genome v. GRCh38, followed by processing with CellRanger (10x Genomics, v2.0) to obtain feature-barcode matrices. Raw count matrices were analyzed using the R package Seurat v. 3.1.34[43]. The matrices were filtered for genes expressed in at least 10 cells and cells that expressed at least 1000 genes. The SCTransform function in Seurat was applied to each Seurat object separately for data normalization and transformation, followed by the application of DoubletFinder v. 2.0.28[44] to each Seurat object separately to remove doublets (assuming that the doublet rate in each sample was 3.9%). Next, all the Seurat objects were merged and filtered by removing cell barcodes with <1000 expressed genes, >7500 expressed genes or >30% reads mapping to mitochondrial genes. The SCTransform function from the Seurat package

was applied to regress out the mitochondrial read percentage per cell. Subsequently, data integration was performed using the R package Harmony v. 1.04[45]. After data normalization and integration, cell cycle scoring was performed per cell, data were filtered for singlets, and SCTransform was again applied to regress out the mitochondrial read percentage and cell cycle scores, followed by data integration of this subset as described above.

Malignant cell identification and CNV inference

To identify malignant cells, two gene sets specific for melanoma were used; these gene sets were acquired from Tirosh et al.[46] (Extended Data Table 4) and Rambow et al.[34] (Extended Data Table 5). The gene activity of these two gene sets was scored using the R package AUCell v.1.6.14[47]. Moreover, we calculated the copy number variation (CNV) based on scRNA-seq data by using the R package HoneyBADGER v. 0.14[48]. The input for HoneyBADGER was the count matrix from the "RNA" assay from the integrated Seurat object of all cells. The reference for normal cells was immune cells, which were also identified by AUCell using the immune gene set from Jerby-Arnon et al.[49]. The mean CNV score was calculated as follows:

$$\text{CNV score} = \frac{\sum_i |G_{\text{cnv},i}|}{n},$$

where G = gene and i= cell.

Next, the mean CNV score was correlated with Tirosh et al.[46] and Rambow et al.[34] gene set activity. Based on the strength of the correlation, the gene set was used for further data analysis for malignant cells. The subsets of malignant cells were subjected to SCTransform (regressing out the mitochondrial read percentage and cell cycle scores) and Harmony integration followed by Seurat clustering. The number of dimensions for clustering was chosen based on Harmony embedding clustering; the cutoff was driven by the identification of clear variation in embeddings across the cells. The activity of different gene expression sets was quantified using AUCell[47].

Statistical analysis

Statistical analysis was performed using GraphPad 7.0. Unless otherwise specified, graphs depict the mean or median ± SD or SEM. Differences between two groups were evaluated using the unpaired Mann-Whitney test or chi-square test. Kaplan-Meier survival curves were assessed to calculate progression-free survival using the log-rank test. The results were considered statistically significant when $P < 0.05$ (*), $P < 0.01$ (**) or $P < 0.001$ (***). Heatmaps summarizing IFN-γ^+ or TNF-α^+ $CD8^+$ T cell responses or IHC signals as percentages of tissue area were used. Receiver operator characteristic (ROC) curves were used to determine the thresholds identifying high vs low expression in IHC analysis.

References

1 Dunn, G. P., Bruce, A. T., Ikeda, H., Old, L. J. & Schreiber, R. D. Cancer immunoediting: from immunosurveillance to tumor escape. *Nat Immunol* **3**, 991-998, doi:10.1038/ni1102-991 (2002).

2 Schreiber, R. D., Old, L. J. & Smyth, M. J. Cancer immunoediting: integrating immunity's roles in cancer suppression and promotion. *Science* **331**, 1565-1570, doi:10.1126/science.1203486 (2011).

3 Knuth, A., Wolfel, T., Klehmann, E., Boon, T. & Meyer zum Buschenfelde, K. H. Cytolytic T-cell clones against an autologous human melanoma: specificity study and definition of three antigens by immunoselection. *Proc Natl Acad Sci U S A* **86**, 2804-2808 (1989).

4 Kawakami, Y. *et al.* Recognition of shared melanoma antigens in association with major HLA-A alleles by tumor infiltrating T lymphocytes from 123 patients with melanoma. *J Immunother* **23**, 17-27, doi:10.1097/00002371-200001000-00004 (2000).

5 Germeau, C. *et al.* High frequency of antitumor T cells in the blood of melanoma patients before and after vaccination with tumor antigens. *J Exp Med* **201**, 241-248, doi:10.1084/jem.20041379 (2005).

6 Coulie, P. G. *et al.* Precursor frequency analysis of human cytolytic T lymphocytes directed against autologous melanoma cells. *Int J Cancer* **50**, 289-297, doi:10.1002/ijc.2910500220 (1992).

7 Tumeh, P. C. *et al.* PD-1 blockade induces responses by inhibiting adaptive immune resistance. *Nature* **515**, 568-571, doi:10.1038/nature13954 (2014).

8 Herbst, R. S. *et al.* Predictive correlates of response to the anti-PD-L1 antibody MPDL3280A in cancer patients. *Nature* **515**, 563-567, doi:10.1038/nature14011 (2014).

9 Burnet, F. M. Immunological surveillance in neoplasia. *Transplant Rev* **7**, 3-25 (1971).

10 Landsberg, J. *et al.* Melanomas resist T-cell therapy through inflammation-induced reversible dedifferentiation. *Nature* **490**, 412-416, doi:10.1038/nature11538 (2012).

11 Effern, M. *et al.* Adoptive T Cell Therapy Targeting Different Gene Products Reveals Diverse and Context-Dependent Immune Evasion in Melanoma. *Immunity* **53**, 564-580 e569, doi:10.1016/j.immuni.2020.07.007 (2020).

12 Holzel, M., Bovier, A. & Tuting, T. Plasticity of tumour and immune cells: a source of heterogeneity and a cause for therapy resistance? *Nat Rev Cancer* **13**, 365-376, doi:10.1038/nrc3498 (2013).

13 Holzel, M. & Tuting, T. Inflammation-Induced Plasticity in Melanoma Therapy and Metastasis. *Trends Immunol* **37**, 364-374, doi:10.1016/j.it.2016.03.009 (2016).

14 Boiko, A. D. *et al.* Human melanoma-initiating cells express neural crest nerve growth factor receptor CD271. *Nature* **466**, 133-137, doi:10.1038/nature09161 (2010).

15 Jager, E. *et al.* Immunoselection in vivo: independent loss of MHC class I and melanocyte differentiation antigen expression in metastatic melanoma. *Int J Cancer* **71**, 142-147, doi:10.1002/(sici)1097-0215(19970410)71:2<142::aid-ijc3>3.0.co;2-0 (1997).

16 Perez-Guijarro, E. *et al.* Multimodel preclinical platform predicts clinical response of melanoma to immunotherapy. *Nat Med* **26**, 781-791, doi:10.1038/s41591-020-0818-3 (2020).

17 Lee, J. H. *et al.* Transcriptional downregulation of MHC class I and melanoma de-differentiation in resistance to PD-1 inhibition. *Nat Commun* **11**, 1897, doi:10.1038/s41467-020-15726-7 (2020).

18 Mehta, A. *et al.* Immunotherapy Resistance by Inflammation-Induced Dedifferentiation. *Cancer Discov* **8**, 935-943, doi:10.1158/2159-8290.CD-17-1178 (2018).

19 Kvistborg, P. *et al.* Anti-CTLA-4 therapy broadens the melanoma-reactive CD8+ T cell response. *Sci Transl Med* **6**, 254ra128, doi:10.1126/scitranslmed.3008918 (2014).
20 Coulie, P. G., Van den Eynde, B. J., van der Bruggen, P. & Boon, T. Tumour antigens recognized by T lymphocytes: at the core of cancer immunotherapy. *Nat Rev Cancer* **14**, 135-146, doi:10.1038/nrc3670 (2014).
21 Chen, Y. T. *et al.* Identification of multiple cancer/testis antigens by allogeneic antibody screening of a melanoma cell line library. *Proc Natl Acad Sci U S A* **95**, 6919-6923, doi:10.1073/pnas.95.12.6919 (1998).
22 Schumacher, T. N. & Schreiber, R. D. Neoantigens in cancer immunotherapy. *Science* **348**, 69-74, doi:10.1126/science.aaa4971 (2015).
23 Hua, C. *et al.* Association of Vitiligo With Tumor Response in Patients With Metastatic Melanoma Treated With Pembrolizumab. *JAMA Dermatol* **152**, 45-51, doi:10.1001/jamadermatol.2015.2707 (2016).
24 Yeh, S. *et al.* Ocular and systemic autoimmunity after successful tumor-infiltrating lymphocyte immunotherapy for recurrent, metastatic melanoma. *Ophthalmology* **116**, 981-989 e981, doi:10.1016/j.ophtha.2008.12.004 (2009).
25 Gogas, H. *et al.* Prognostic significance of autoimmunity during treatment of melanoma with interferon. *N Engl J Med* **354**, 709-718, doi:10.1056/NEJMoa053007 (2006).
26 Larkin, J. *et al.* Combined Nivolumab and Ipilimumab or Monotherapy in Untreated Melanoma. *N Engl J Med* **373**, 23-34, doi:10.1056/NEJMoa1504030 (2015).
27 Eisenhauer, E. A. *et al.* New response evaluation criteria in solid tumours: revised RECIST guideline (version 1.1). *Eur J Cancer* **45**, 228-247, doi:10.1016/j.ejca.2008.10.026 (2009).
28 Wolchok, J. D. *et al.* Guidelines for the evaluation of immune therapy activity in solid tumors: immune-related response criteria. *Clin Cancer Res* **15**, 7412-7420, doi:10.1158/1078-0432.CCR-09-1624 (2009).
29 Robert, C. *et al.* Pembrolizumab versus Ipilimumab in Advanced Melanoma. *N Engl J Med* **372**, 2521-2532, doi:10.1056/NEJMoa1503093 (2015).
30 Matsushita, H. *et al.* Cancer exome analysis reveals a T-cell-dependent mechanism of cancer immunoediting. *Nature* **482**, 400-404, doi:10.1038/nature10755 (2012).
31 Rosenberg, S. A. & Restifo, N. P. Adoptive cell transfer as personalized immunotherapy for human cancer. *Science* **348**, 62-68, doi:10.1126/science.aaa4967 (2015).
32 Rosenberg, S. A. *et al.* Durable complete responses in heavily pretreated patients with metastatic melanoma using T-cell transfer immunotherapy. *Clin Cancer Res* **17**, 4550-4557, doi:10.1158/1078-0432.CCR-11-0116 (2011).
33 Tsoi, J. *et al.* Multi-stage Differentiation Defines Melanoma Subtypes with Differential Vulnerability to Drug-Induced Iron-Dependent Oxidative Stress. *Cancer Cell* **33**, 890-904 e895, doi:10.1016/j.ccell.2018.03.017 (2018).
34 Rambow, F. *et al.* New Functional Signatures for Understanding Melanoma Biology from Tumor Cell Lineage-Specific Analysis. *Cell Rep* **13**, 840-853, doi:10.1016/j.celrep.2015.09.037 (2015).
35 Hoek, K. S. *et al.* In vivo switching of human melanoma cells between proliferative and invasive states. *Cancer Res* **68**, 650-656, doi:10.1158/0008-5472.CAN-07-2491 (2008).
36 Verfaillie, A. *et al.* Decoding the regulatory landscape of melanoma reveals TEADS as regulators of the invasive cell state. *Nat Commun* **6**, 6683, doi:10.1038/ncomms7683 (2015).
37 Sun, C. *et al.* Reversible and adaptive resistance to BRAF(V600E) inhibition in melanoma. *Nature* **508**, 118-122, doi:10.1038/nature13121 (2014).

38 Kanik, A. B., Yaar, M. & Bhawan, J. p75 nerve growth factor receptor staining helps identify desmoplastic and neurotropic melanoma. *J Cutan Pathol* **23**, 205-210, doi:10.1111/j.1600-0560.1996.tb01468.x (1996).

39 Eggermont, A. M. M., Robert, C. & Ribas, A. The new era of adjuvant therapies for melanoma. *Nat Rev Clin Oncol* **15**, 535-536, doi:10.1038/s41571-018-0048-5 (2018).

40 Eggermont, A. M. M., Robert, C. & Suciu, S. Adjuvant Pembrolizumab in Resected Stage III Melanoma. *N Engl J Med* **379**, 593-595, doi:10.1056/NEJMc1807505 (2018).

41 Huang, A. C. *et al.* T-cell invigoration to tumour burden ratio associated with anti-PD-1 response. *Nature* **545**, 60-65, doi:10.1038/nature22079 (2017).

42 Bankhead, P. *et al.* QuPath: Open source software for digital pathology image analysis. *Sci Rep* **7**, 16878, doi:10.1038/s41598-017-17204-5 (2017).

43 Stuart, T. *et al.* Comprehensive Integration of Single-Cell Data. *Cell* **177**, 1888-1902 e1821, doi:10.1016/j.cell.2019.05.031 (2019).

44 McGinnis, C. S., Murrow, L. M. & Gartner, Z. J. DoubletFinder: Doublet Detection in Single-Cell RNA Sequencing Data Using Artificial Nearest Neighbors. *Cell Syst* **8**, 329-337 e324, doi:10.1016/j.cels.2019.03.003 (2019).

45 Korsunsky, I. *et al.* Fast, sensitive and accurate integration of single-cell data with Harmony. *Nat Methods* **16**, 1289-1296, doi:10.1038/s41592-019-0619-0 (2019).

46 Tirosh, I. *et al.* Dissecting the multicellular ecosystem of metastatic melanoma by single-cell RNA-seq. *Science* **352**, 189-196, doi:10.1126/science.aad0501 (2016).

47 Aibar, S. *et al.* SCENIC: single-cell regulatory network inference and clustering. *Nat Methods* **14**, 1083-1086, doi:10.1038/nmeth.4463 (2017).

48 Fan, J. *et al.* Linking transcriptional and genetic tumor heterogeneity through allele analysis of single-cell RNA-seq data. *Genome Res* **28**, 1217-1227, doi:10.1101/gr.228080.117 (2018).

49 Jerby-Arnon, L. *et al.* A Cancer Cell Program Promotes T Cell Exclusion and Resistance to Checkpoint Blockade. *Cell* **175**, 984-997 e924, doi:10.1016/j.cell.2018.09.006 (2018).

Acknowledgments

The authors thank Caroline Dietrich and Martina Kurz from the Clinical Trials Unit, Kantonsspital St.Gallen, for the excellent management of the St.Gallen patient cohort. The authors also thank Simone Golling, Institute of Pathology at the Kantonsspital St.Gallen, and Romina Zarbl, University of Bonn, for providing excellent technical support. We also thank the NGS Core Facility of the University Hospital Bonn. We appreciate the support of the University of Zurich Research Priority Program (URPP). The manuscript was edited for proper English language, grammar, punctuation, spelling, and overall style by one or more of the highly qualified native English speaking editors at SNAS.

Funding

This study was funded in part by grant #PP00P3_157448 from the Swiss National Science Foundation and grant #18A042 from the Novartis Foundation for Medical Biological Research (both to L.F.). The study coordination of the St. Gallen patient cohort was supported by a grant from the Forschungsförderung of the Kantonsspital St Gallen. M.H. was supported by the Deutsche Forschungsgemeinschaft (DFG, German Research Foundation) under Germany's Excellence Strategy - EXC2151 - 390873048. M.v.d.B was funded by the Swiss National Science Foundation (CRSII5_177208 and 310030_175565) and the University of Zurich (University Research Priority Program "Translational Cancer Research").

Author contributions

L.F., S.S.R., O.T.P. designed the study, discussed data and wrote the paper; S.S.R., O.T.P., M.-T.A. and S.N.F. performed experiments, analyzed and discussed data. J.P., E. L., F.R., G.B., O.B. performed experiments and bioinformatics analyses and discussed data. F.B., O.H.A., M.-T.A., S.D., R.N., M.F. managed the SG patient cohort and collected patient material. W.J. provided

patient material and discussed data. J.M., R.D., and M.P.L. provided patient data and material for the adjuvant Zurich Cohort. T.B., T.M., M.M. provided patient material. J.L., D.D., D.B., M.v.d.B., A.C., C.G., M.P.L., B.L. discussed data. T.T., M.H., J.-C. M discussed data and provided support to develop the manuscript.

Competing financial interests

L.F. discloses grants from the Swiss National Science Foundation, Swiss Cancer League, Hookipa Pharma, and Novartis Foundation as well as advisory roles for Novartis, Sanofi and Bristol-Myers Squibb. T.B. has a research agreement with Bristol-Myers Squibb.

Data and materials availability

scRNA-seq data will be available. Further information and requests for resources and reagents should be directed to and will be fulfilled by the lead investigator, Lukas Flatz (lukas.flatz@med.uni-tuebingen.de).

Extended Data Figures and Tables

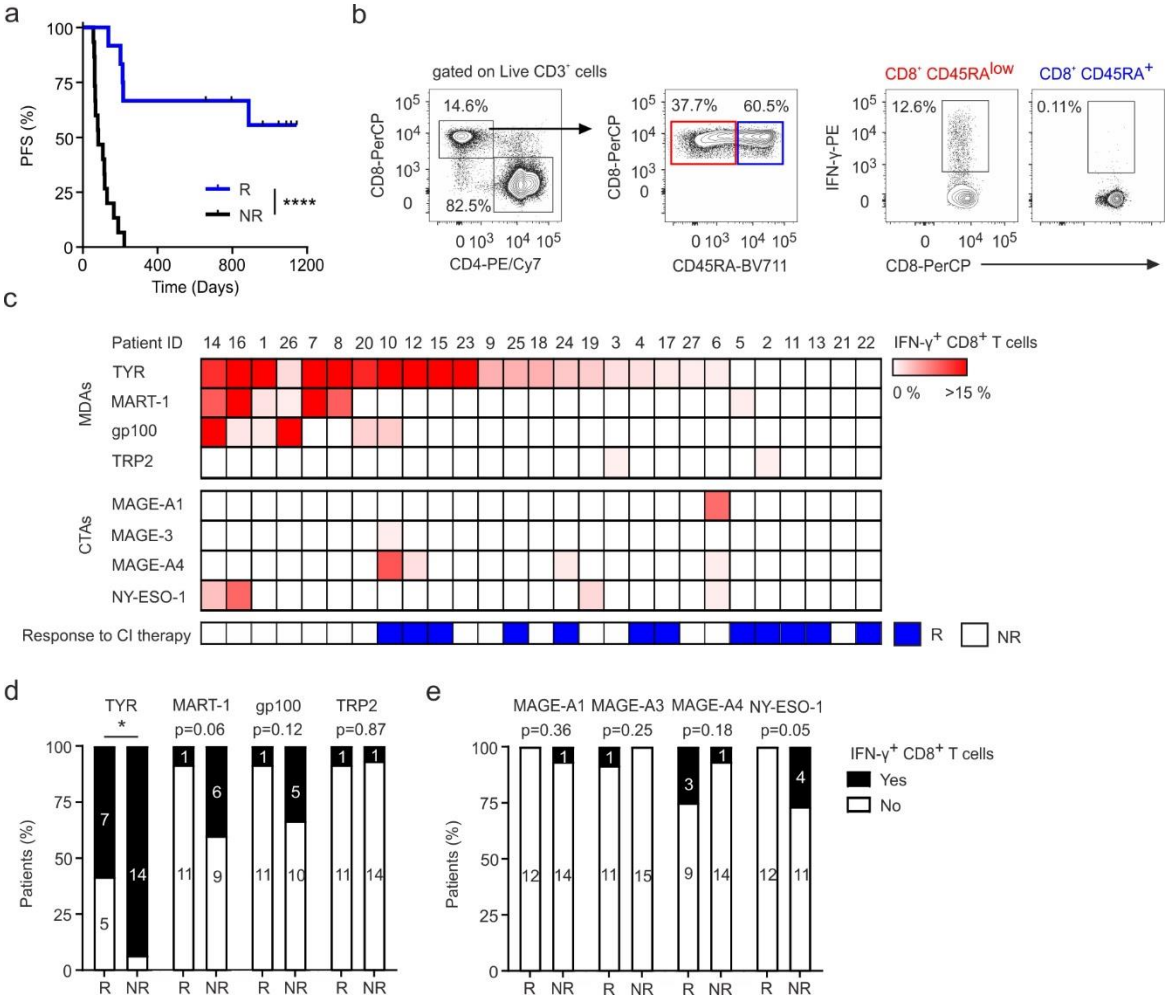

Extended Data Figure 1. Pre-existing MDA- and CTA-specific IFN-γ$^+$ CD8$^+$ T cells in melanoma patients receiving checkpoint inhibitor therapy. a, Progression-free survival of patients with stage IV melanoma in the St. Gallen (SG) cohort. Clinical responders (R; complete or partial response; n=12) and nonresponders (NR; progressive disease; n=15) to checkpoint inhibitor therapy. **b-e,** PBMCs were obtained from SG cohort patients prior to checkpoint inhibitor therapy and stimulated in vitro with overlapping 15-mer peptide pools specific for the melanocyte differentiation antigens (MDAs) TYR, MART-1, gp100, and TRP2 and the cancer testis antigens (CTAs) MAGE-A1, MAGE-A3, MAGE-A4, and NY-ESO-1. **b,** The FACS gating strategy is shown. Cytokine-producing cells were detected within the antigen-experienced CD45RA^{low} CD8$^+$ T cell population. **c,** Heatmaps summarizing the frequencies of IFN-γ-producing CD8$^+$ T cells for the indicated antigens. The color scale represents the frequency of IFN-γ$^+$ CD3$^+$ CD8$^+$ CD45RA^{low} T cells. **d-e,** Proportions of R and NR with IFN-γ$^+$ CD8$^+$ T cell responses against MDAs (**d**) and CTAs (**e**) after checkpoint inhibitor therapy. Statistical analysis was performed using log-rank (a) and chi-square tests (d and e); *P < 0.05, **P < 0.01, ***P < 0.001.

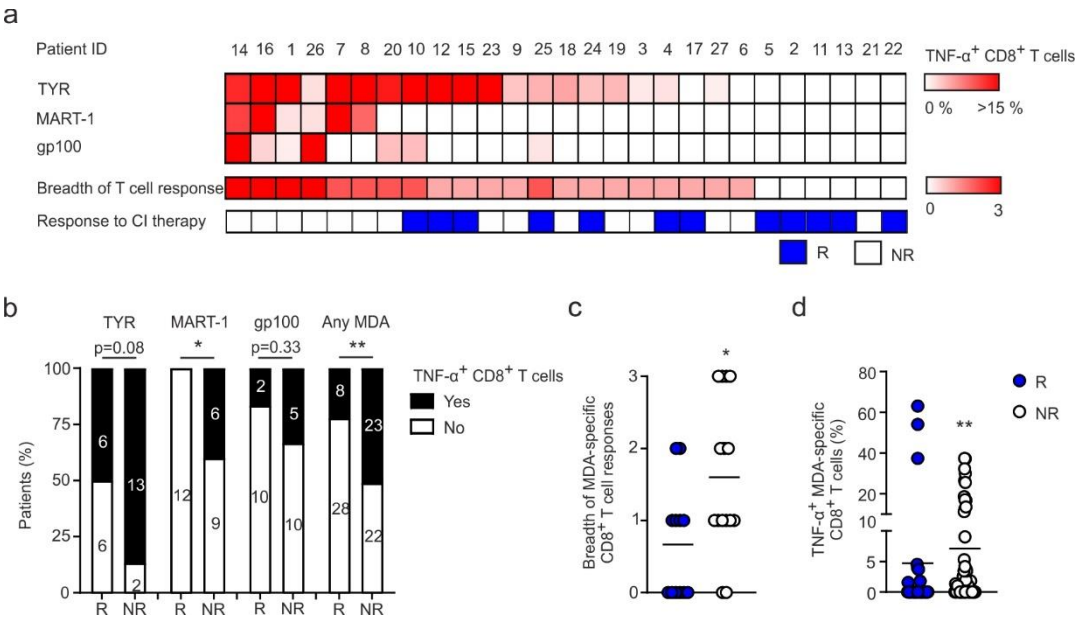

Extended Data Figure 2. Pre-existing MDA-specific TNF-α⁺ CD8⁺ T cells in melanoma patients receiving checkpoint inhibitor therapy. a, Heatmaps summarizing TNF-α⁺ CD8⁺ T cells in the SG cohort for the indicated antigens. The color scale represents the frequency of TNF-α⁺ CD3⁺ CD8⁺ CD45RA^{low} T cells. The breadth of the CD8⁺ T cell response was defined as the number of individual MDAs recognized, as indicated by the detection of TNF-α⁺ CD8⁺ T cell responses, ranging from 0 (none) to 3 (all). **b,** Proportions of R and NR with TNF-α⁺ MDA-specific CD8⁺ T cell responses after checkpoint inhibitor therapy. **c,** Summary of the breadth of MDA-specific CD8⁺ T cells in R and NR as shown for individual patients as shown in panel a. **d,** Frequencies of TNF-α⁺ CD8⁺ T cells against any MDA (TYR, MART-1 or gp100) in R vs NR. Dots represent individual patients, and lines indicate mean values (c and d). Statistical analysis was performed using the chi-square test (b) and Mann-Whitney test (c and d); *P < 0.05, **P < 0.01, ***P < 0.001.

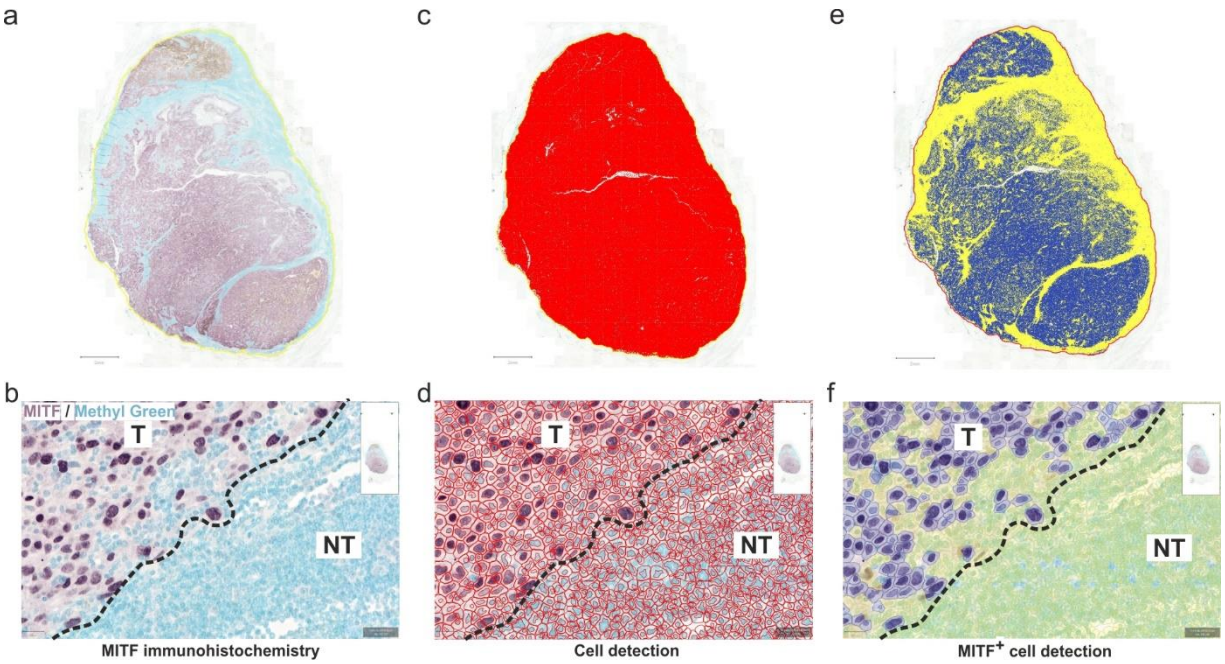

Extended Data Figure 3. Quantitative digital morphometry of enzymatic IHC using QuPath: image analysis strategy. a, Whole-slide scan of a lymph node metastasis stained for MITF (violet chromogen) with methyl green counterstaining. The selected region of interest for analysis is indicated (yellow outline). **b**, Detail showing MITF$^+$ tumor cells (violet nuclei) and MITF$^-$ cells (NT); the dashed line separates tumor (T) and non-tumor (NT) areas (200× magnification). **c**, Cell identification (red mask) on the whole-slide scan using the "Cell detection command". **d**, Detailed results for cell identification (red cellular and nuclear contours) (200× magnification). **e**, Results of cell classification by training a two-way boosted decision tree classifier (blue mask – MITF$^+$ tumor cells; yellow mask – MITF$^-$ cells). **f**, Detail showing the results of cell classification (blue and yellow masks and contours identifying MITF$^+$ tumor cells and MITF$^-$ cells, respectively) (200× magnification).

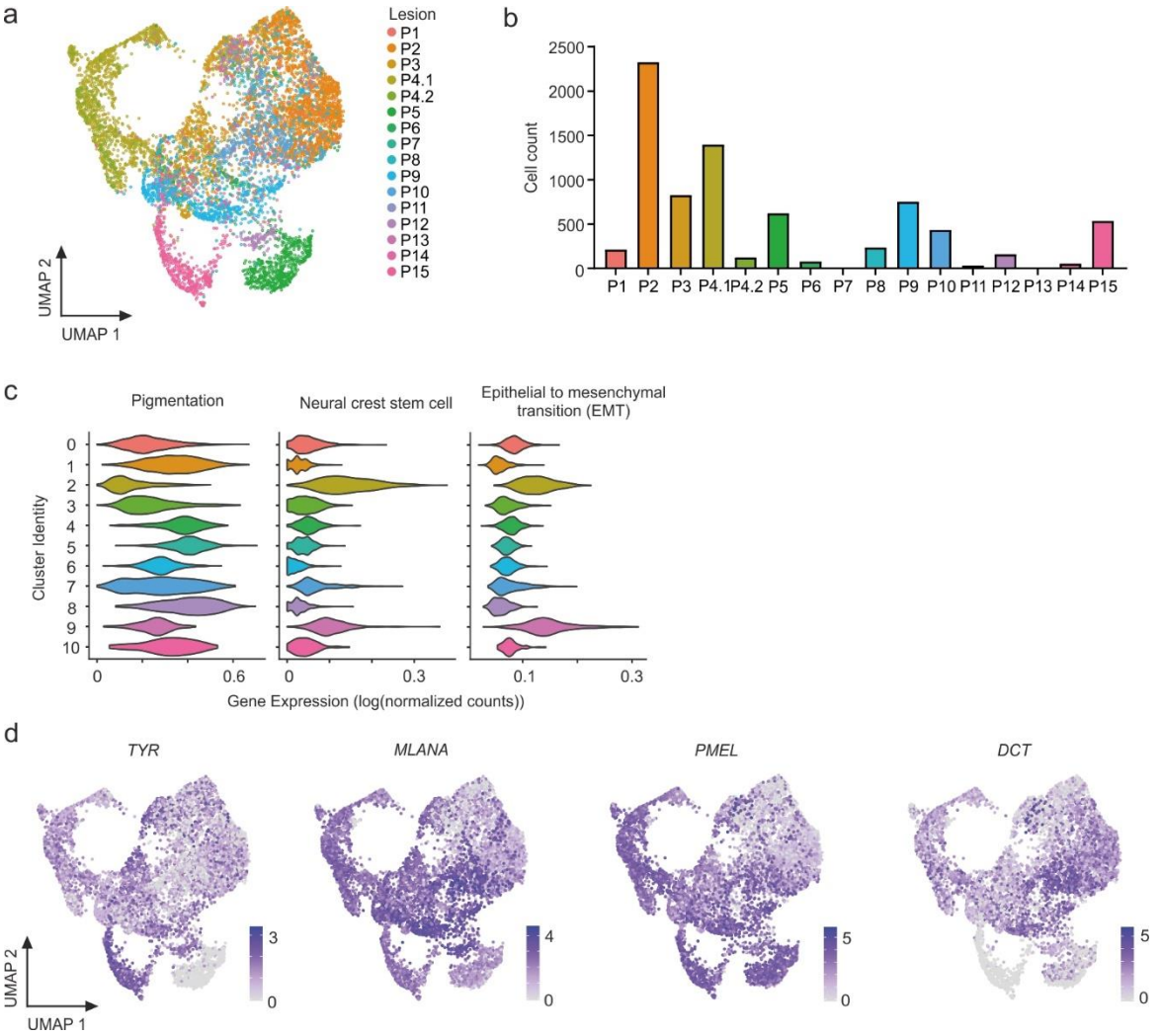

741

742 **Extended Data Figure 4. Transcriptomic analysis revealing tumor cells with a dedifferentiated**
743 **phenotype. a,** Single-cell RNA sequencing of tumor cells from metastatic lesions obtained from 15 stage
744 III and IV melanoma patients (Leuven cohort). UMAP plot displays individual lesion assignment to the
745 assigned clusters as shown in Fig. 3a. **b**, Bar graph indicating the number of cells obtained from each lesion.
746 **c**, Violin plots based on the Rambow et al. (2015)[34] gene signatures for pigmentation, neural crest stem
747 cells (NCSCs) and epithelial-mesenchymal transition (EMT). Tumor cells in cluster 2, 3, 7 and 9 exhibit a
748 dedifferentiated phenotype **d,** UMAP plots showing the gene expression of *TYR*, *MLANA* (MART-1),
749 *PMEL* (gp100) and *DCT* (TRP2).

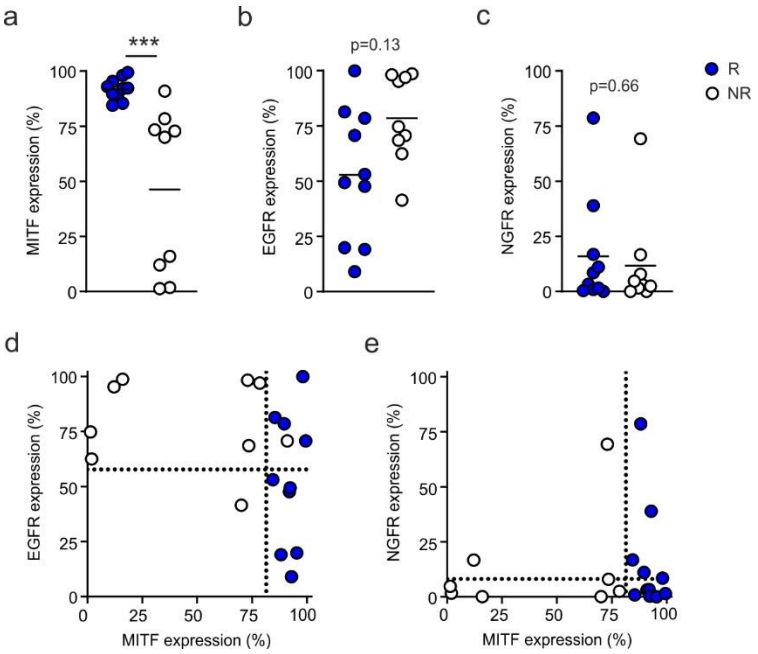

Extended Data Figure 5. The dedifferentiated tumor phenotype is associated with the clinical response to checkpoint inhibitor treatment. a-c, Frequencies of melanoma cells stained positive for MITF, EGFR or NGFR in responders (R) and nonresponders (NR). **d-e,** The dedifferentiated phenotype was defined as **d,** $MITF^{low}$ $EGFR^{high}$ or **e,** $MITF^{low}$ $NGFR^{high}$ as defined by threshold values from ROC curves for each individual protein (dotted lines). Dots represent individual patients (a-e) and lines indicate mean values (a-c). Statistical analysis was performed using the Mann-Whitney test; *P < 0.05, **P < 0.01, ***P < 0.001.

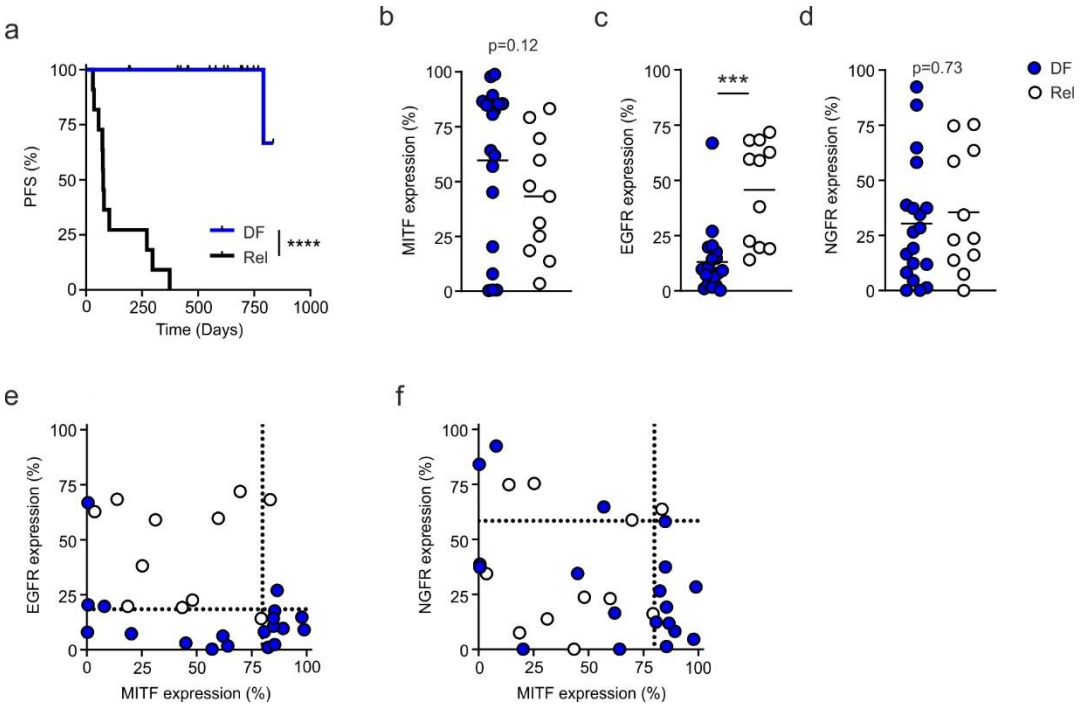

Extended Data Figure 6. A dedifferentiated tumor phenotype predicts the clinical response to adjuvant checkpoint inhibitor therapy. a, Progression-free survival of patients with stage III melanoma in the Zurich (ZH) adjuvant anti-PD-1 cohort. Disease-Free patients (DF; R; n=19) and patients who experienced relapse (Rel; n=11) were determined at the first PET-CT scan within 3 months after start of therapy. **e-f,** Tumor biopsies were obtained before initiation of treatment. and frequencies of melanoma cells stained positive for MITF, EGFR or NGFR in the DF and Rel groups. **e-f,** The dedifferentiated phenotype was defined as **e,** $MITF^{low}$ $EGFR^{high}$ or **f,** $MITF^{low}$ $NGFR^{high}$ as defined by threshold values from ROC curves for each individual protein (dotted lines). Dots represent individual patients (b-f) and lines indicate mean values (b-d).Statistical analysis was performed using the log-rank (a) and Mann-Whitney tests (d-g); *P < 0.05, **P < 0.01, ***P < 0.001.

Extended Data Table 1. Patient characteristics of the St.Gallen (SG) cohort

Characteristic	Responders (N = 12, 44 %)	Nonresponders (N = 15, 56 %)
Age at start of treatment - years		
Median	69	69
Range	41-81	47-86
Sex - no. of patients (%)		
Female	4 (33.3)	10 (66.7)
Male	8 (66.7)	5 (33.3)
Histological type (primary tumor) - no. of patients (%)		
Superficial spreading	5 (41.7)	7 (46.6)
Nodular	3 (25)	1 (6.7)
Acral lentiginous	1 (8.3)	0 (0)
Mucosal lentiginous	0 (0)	1 (6.7)
Uveal	1 (8.3)	3 (20)
Unknown primary	2 (16.7)	3 (20)
BRAF mutation - no. of patients (%)		
No	8 (66.7)	10 (66.7)
Yes	4 (33.3)	5 (33.3)
CRP levels at start of therapy - mg/L		
Median	1	5
Range	0-19	0-114
WBC at start of therapy - g/L		
Median	7.7	7.3
Range	3-13.9	3.4-11
Lymphocytes at start of therapy - g/L		
Median	1.6	1.2
Range	0.4-2.9	0.6-3
Granulocytes at start of therapy - g/L		
Median	4.9	5.4
Range	2.2-12.1	1.8-8.7
Checkpoint inhibitor therapy - no. of patients (%)		
pembrolizumab	9 (75)	12 (80)
ipilimumab + nivolumab	3 (25)	3 (20)
Progression-free survival - days*		
Median	481	107
Range	137-878	56-222
Overall survival - days†		
Median	615	371
Range	256-931	107-908

* Progression-free survival was calculated from the date of first dose of CI to the date of progression or censoring of data

† Overall survival was calculated from the date of first dose of CI to the date of death or censoring of data

776 **Extended Data Table 2. Patient characteristics of the Leuven cohort**

Patient number	Orig.ident	Tissue	Library type	Stage
P1	sc5rCMA070	Subcutis	5′ GEX	IV
P2	scrCMA036	Subcutis	3′ GEX	IV
P3	scrCMA038	Lymph node	3′ GEX	IV
P4.1	scrCMA040	Skin	3′ GEX	IV
P4.2	scrCMA041	Skin	3′ GEX	IV
P5	scrCMA054	Lymph node	3′ GEX	IV
P6	scrCMA055	Lymph node	3′ GEX	IIIC
P7	scrCMA068	Subcutis	3′ GEX	IV
P8	scrCMA076	Lymph node	3′ GEX	IV
P9	scrCMA087	Lymph node	3′ GEX	IV
P10	scrCMA090	Subcutis	3′ GEX	IV
P11	scrCMA093	Lymph node	3′ GEX	IIIC
P12	scrCMA094	Lymph node	3′ GEX	IV
P13	scrCMA109	Skin	3′ GEX	IIIC
P14	scrCMA119	Lymph node	3′ GEX	IIID
P15	scrCMA120	Skin	3′ GEX	IV

777

Extended Data Table 3. Patient characteristics of the Zurich (ZH) Cohort

Characteristic	Disease-Free (N = 19, 63%)	Relapse (N = 11, 37%)
Age at start of treatment - years		
Median	62	67
Range	22-78	35-87
Sex - no. of patients (%)		
Female	9 (47.4)	7 (63.6)
Male	10 (52.6)	4 (36.4)
BRAF mutation - no. of patients (%)		
No	14 (73.7)	3 (27.3)
Yes	5 (26.3)	8 (72.7)
Progression-free survival - days*		
Median	615	77
Range	191-835	31-373
Overall survival - days†		
Median	615	540
Range	191-856	170-895

* Progression-free survival was calculated from the date of first dose of CI to the date of progression or censoring of data

† Overall survival was calculated from the date of first dose of CI to the date of death or censoring of data

Extended Data Table 4. Gene signatures based on Tsoi et al.[33]

Undifferentiated	Neural crest- like	Transitory	Melanocytic
AJUBA	*VIT*	*XYLT1*	*CCDC171*
TOR4A	*VIPR1*	*TSPAN7*	*CFAP61*
MARCH4	*VEGFC*	*SOD3*	*ZDHHC11B*
ZDHHC2	*TWIST2*	*SCRG1*	*VEPH1*
ZNF467	*TNFRSF12A*	*SORL1*	*TNFRSF14*
ZNF185	*TPM1*	*SEMA3E*	*TDRD3*
ZIC2	*TPBG*	*SELENBP1*	*TPPP*
VASN	*TLE4*	*RNASE1*	*TRIM63*
UCP2	*TOX2*	*RAPGEF4*	*TRPM1*
GALNT6	*TLR4*	*PCDH7*	*TTC39A*
TNFAIP2	*THSD4*	*PRSS33*	*TSPAN10*
TNFSF18	*STX1A*	*PCSK6*	*SLC7A8*
TMEM40	*SYT1*	*PLBD1*	*SLC16A6*
TMEM200A	*SYNPO*	*NELL1*	*SLAMF7*
TMEM184A	*STRA6*	*NPR1*	*SEMA6A*
TBL1X	*STC2*	*MCAM*	*RUNX3*
TRERF1	*SPRED3*	*MMP15*	*RNF144B*
TOX	*SPOCD1*	*MAMDC2*	*RNLS*
TBC1D2	*SPOCK1*	*LSAMP*	*RGS12*
SFN	*SLC2A1*	*LRRTM4*	*PYCARD*
SAMD12	*SLC16A2*	*GDF11*	*PRUNE2*
SAMD11	*SLC14A1*	*FXYD3*	*PRKCB*
SOX9	*SLC12A8*	*EBF3*	*PRDM7*
SLC8A1	*SMAGP*	*COL11A2*	*KCNAB2*
SLC38A4	*SLIT2*	*COL9A1*	*OCA2*
SLC16A14	*SDK1*	*CX3CL1*	*NR4A3*
SCN5A	*STAC*	*BCHE*	*NAV2*
SCNN1A	*SLFN11*	*ANO4*	*MYO1D*
SH3RF2	*S100A2*	*ALDH1A1*	*MAPK4*
SERPINB7	*ROBO4*		*MAT1A*
SLPI	*RAB27B*		*MLANA*
SECTM1	*PKIA*		*LXN*
RUNX2	*PRSS23*		*KCP*
ARHGAP29	*PAPPA*		*IL16*
REN	*PRDM1*		*IL12RB2*
PAWR	*KCNMA1*		*HSD17B14*
PSG9	*KCNN4*		*HMOX1*
PSG5	*PODXL*		*H2AFJ*
PSG4	*PDGFRB*		*GOLGA7B*
PBX1	*PLAUR*		*QPCT*
PLAGL1	*PXDN*		*GFOD1*
PHLDB2	*PTX3*		*GPR143*

PLEKHA6
PDGFC
PLAU
PKP2
PLAC8
PADI3
PITX1
NUAK1
NTNG1
NMT2
MYEOV
MICAL2
MGST1
MECOM
LYPD6B
LAMA5
KISS1
KRT86
KRT81
KRT80
KRT8
KRT7
KRT18
JUP
IL7R
IL4R
IRS1
IGFN1
HES7
GDA
GLIS2
GATA2
GPRC5C
GPRC5A
FMNL1
FOXA1
FLNC
FERMT1
FAT4
FAM196B
ELFN2
EGFR
DSE
DMBT1
NMNAT2
NRP1
NGEF
NEGR1
NRG1
NTN4
MT2A
MT1E
MPP4
LOXL2
LDOC1
LAMB3
JUN
IL31RA
IL11
IL1B
ITGA3
ITGA2
IGFBP6
ID1
INHBA
HRH1
GAS6
GLIPR1
GFRA1
GATA3
GPR176
FZD2
FJX1
FOSL1
FOXF1
FBLIM1
FLNB
FAM83G
FAM20C
FAM171A1
FAM155A
ERRFI1
EFNB2
DPYD
DKK1
DOCK5
CYR61
CLMP
FYB
FAM83H
FAM174B
EPHA5
ENTHD1
DNAJA4
DENND2D
C2orf88
CCL18
CEACAM1
CAPG
CDH3
CDH1
ATP6V0D2
ABCD1
ABCB5
APOLD1
ANKRD30B
ADCY2
ADAM23)

DIO2	*COL13A1*
DOCK2	*COL12A1*
CYP2S1	*COL5A1*
CRIM1	*F2RL2*
CDK15	*C16orf45*
CORO6	*C15orf52*
COLEC10	*C12orf75*
CCDC88C	*CD163L1*
CCDC69	*CAV1*
F3	*CARD10*
F2RL1	*CLCF1*
CLU	*CDH13*
CDYL2	*BMP2*
CITED2	*AXL*
CARD11	*ABCC3*
CPA4	*ARNTL2*
CREB3L1	*ANTXR2*
CNN1	*ANXA1*
CALB2	*AKR1C3*
CDH4	*ARL4C*
BTBD11	
BDNF	
BASP1	
BNC1	
ATP8B1	
ABCG2	
ARMC4	
ANKRD1	
AR	
AMIGO2	
ADAMTSL1	
ACSL5	

Extended Data Table 5. Gene signatures based on Rambow et al.[34]

Pigmentation	HALLMARK_EMT	NSCS
TYR	*ABI3BP*	*IGF1*
SLC45A2	*ACTA2*	*CADM1*
PMEL	*ADAM12*	*VCAN*
SLC24A5	*ANPEP*	*ADAMTS4*
S100B	*APLP1*	*PDGFB*
MLANA	*AREG*	*ITGA6*
GPR143	*BASP1*	*SYT11*
MLPH	*BDNF*	*COL4A1*
RAB38	*BGN*	*AQP1*
MITF	*BMP1*	*ATP1B2*
TYRP1	*CADM1*	*ADGB*
DCT	*CALD1*	*TMEM176B*
RAB27A	*CALU*	*SLC22A17*
EDNRB	*CAP2*	*NRXN1*
KIT	*CAPG*	*MATN2*
TRPM1	*CD44*	*GFRA1*
	CD59	*MPZ*
	CDH11	*NGFR*
	CDH2	*PRIMA1*
	CDH6	*LAMCC1*
	COL11A1	*RSPO3*
	COL12A1	*ITGA1*
	COL16A1	*THBS2*
	COL1A1	*NLGN3*
	COL1A2	*GFRA3*
	COL3A1	*S100A4*
	COL4A1	*CNN3*
	COL4A2	*ANXA1*
	COL5A1	*SLITRK6*
	COL5A2	*A2M*
	COL5A3	*COL1A1*
	COL6A2	*L1CAM*
	COL6A3	*SEMA3B*
	COL7A1	*GFRA2*
	COL8A2	*ATP1A2*
	COMP	*IL1RAP*
	COPA	*PLAT*
	CRLF1	*SOX10*
	CTGF	*GDNF*
	CTHRC1	*RXRG*
	CXCL1	*MEF2C*
	CXCL12	*TFAP2B*

CXCL6
CYR61
DAB2
DCN
DKK1
DPYSL3
DST
ECM1
ECM2
EDIL3
EFEMP2
ELN
EMP3
ENO2
FAP
FAS
FBLN1
FBLN2
FBLN5
FBN1
FBN2
FERMT2
FGF2
FLNA
FMOD
FN1
FOXC2
FSTL1
FSTL3
FUCA1
FZD8
GADD45A
GADD45B
GAS1
GEM
GJA1
GLIPR1
GLT25D1
GPC1
GPX7
GREM1
HTRA1
ID2
IGFBP2

IGFBP3
IGFBP4
IL15
IL32
IL6
IL8
INHBA
ITGA2
ITGA5
ITGAV
ITGB1
ITGB3
ITGB5
JUN
LAMA1
LAMA2
LAMA3
LAMC1
LAMC2
LEPRE1
LGALS1
LOX
LOXL1
LOXL2
LRP1
LRRC15
LUM
MAGEE1
MATN2
MATN3
MCM7
MEST
MFAP5
MGP
MMP1
MMP14
MMP2
MMP3
MSX1
MXRA5
MYL9
MYLK
NID2
NNMT

NOTCH2
NT5E
NTM
OXTR
PCOLCE
PCOLCE2
PDGFRB
PDLIM4
PFN2
PLAUR
PLOD1
PLOD2
PLOD3
PMEPA1
PMP22
POSTN
PPIB
PRRX1
PRSS2
PTHLH
PTX3
PVR
QSOX1
RGS4
RHOB
SAT1
SCG2
SDC1
SDC4
SERPINE1
SERPINE2
SERPINH1
SFRP1
SFRP4
SGCB
SGCD
SGCG
SLC6A8
SLIT2
SLIT3
SNAI2
SNTB1
SPARC
SPOCK1

SPP1
TAGLN
TFPI2
TGFB1
TGFBI
TGFBR3
TGM2
THBS1
THBS2
THY1
TIMP1
TIMP3
TNC
TNFAIP3
TNFRSF11B
TNFRSF12A
TPM1
TPM2
TPM4
VCAM1
VCAN
VEGFA
VEGFC
VIM
WIPF1
WNT5A

788

Figures

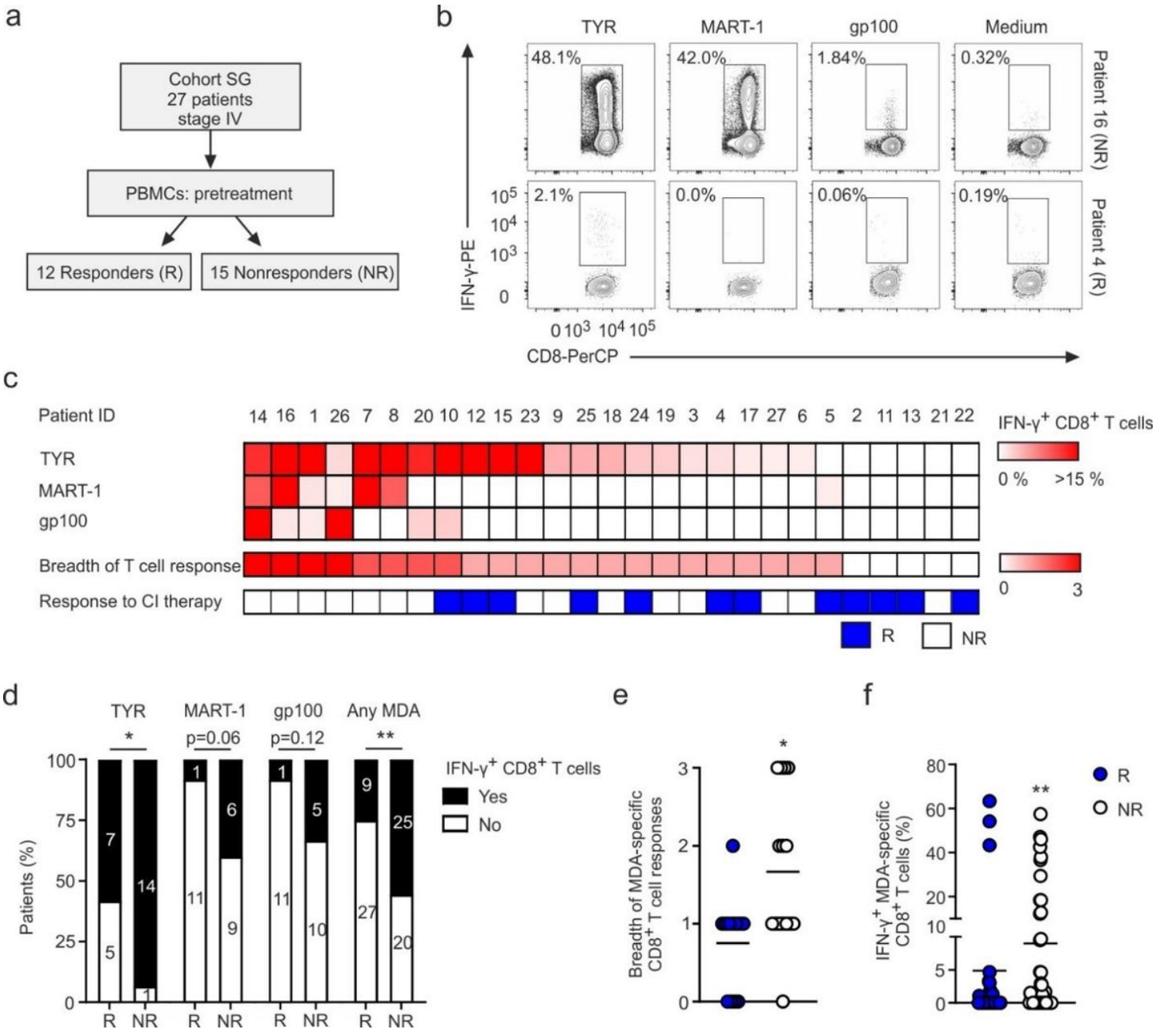

Figure 1

Levels of pre-existing MDA-specific CD8+ T cells in melanoma patients receiving checkpoint inhibitor therapy. a, In the prospective St.Gallen (SG) cohort, peripheral blood mononuclear 2cells (PBMCs) were obtained from 27 patients with stage IV melanoma prior to checkpoint inhibitor therapy. Clinical responders (R; N=12) and nonresponders (NR; N=15) were determined at 12 weeks. b-f, CD8+ T cell responses against the melanocyte differentiation antigens (MDAs) TYR, MART-1 and gp100 after in vitro stimulations of PBMCs with overlapping 15-mer peptide pools for each individual antigen for 10 days as measured by IFN-γ expression. b, Representative FACS plots of samples from patient 16 (NR) and patient

4 (R). c, Heatmaps summarizing the frequency of IFN-γ-producing CD8+ T cells for the indicated antigens. The color scale represents the frequency of IFN-γ+ CD3+ CD8+ CD45RAlow T cells. The breadth of the CD8+ T cell response was defined as the number of the individual IFN-γ+ CD8+ T cells against the MDAs TYR, MART-1 and gp100, as indicated by the detection of IFN-γ+ CD8+ T cell responses, ranging from 0 (none) to 3 (all). d, Proportions of R and NR with MDA-specific CD8+ T cell responses to the individual MDAs or any MDA. e, Summary of the breadth of MDA-specific CD8+ T cells in R and NR as shown for individual patients as shown in panel c. f, Frequencies of IFN-γ+ CD8+ T cells against any MDA (TYR, MART-1 or gp100) in R vs NR. Dots represent individual patients, and lines indicate the mean values (e and f). Statistical analysis was performed using the chi-square test (d) and Mann-Whitney test (e and f); *P < 0.05, **P < 0.01, ***P < 0.001.

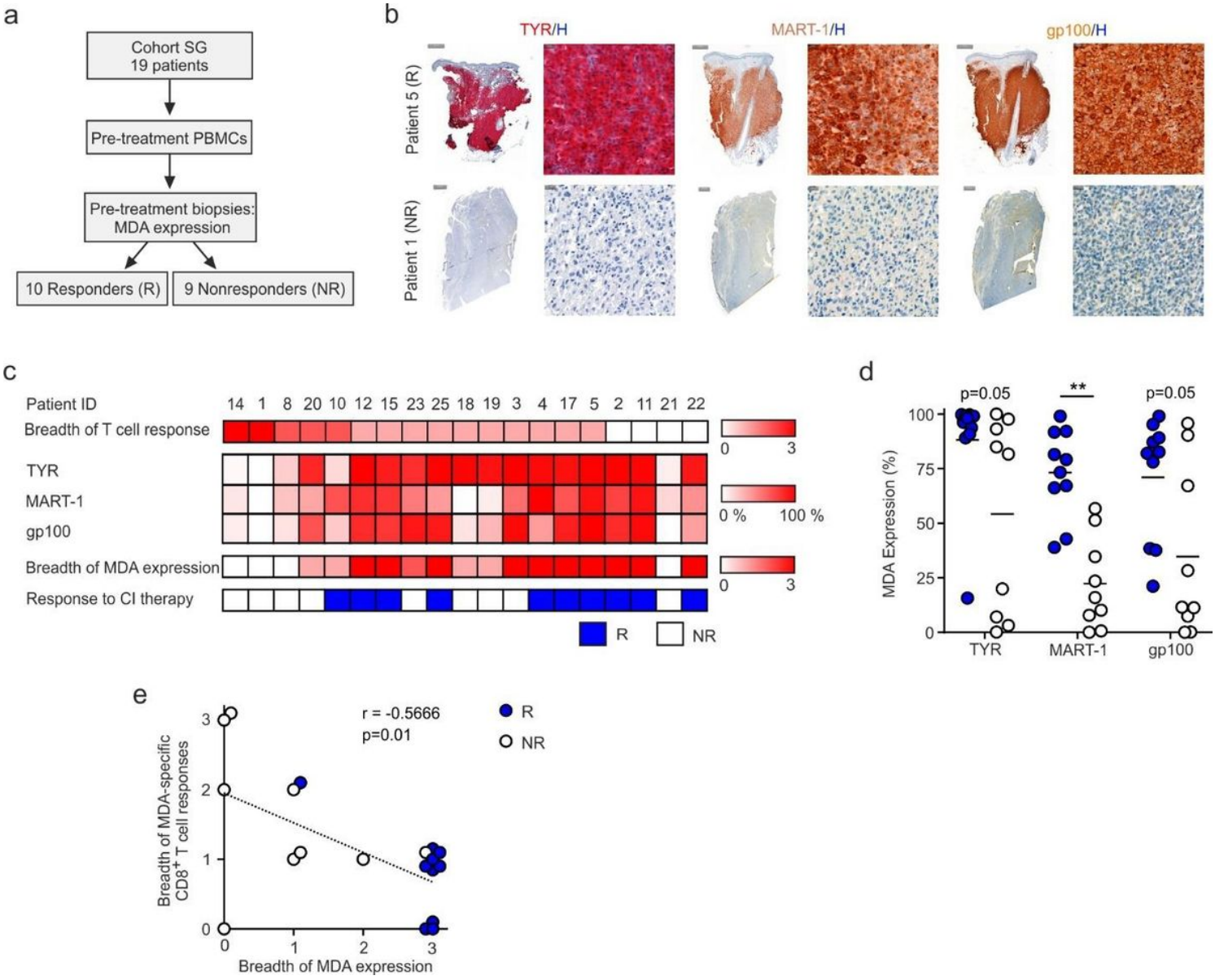

Figure 2

MDA tissue expression inversely correlates with peripheral MDA-specific CD8+ T cells. a,In 19 of the patient from the SG cohort, tumor biopsies obtained before initiation of checkpoint inhibitor therapy and

matched PBMCs from Fig. 1 were analyzed. The expression of the MDAs TYR, MART-1 and gp100 was analyzed using quantitative IHC analysis of biopsy tissue. b, Representative images for the indicated antigens in patient 5 (R) and patient 1 (NR). The frequency of tumor cells expressing each of these antigens was assessed as outlined in Extended Data Figure 3. Hematoxylin (H) staining to identify the cell nucleus. Scale bars are 500 and 2000 μm for the general images (top and bottom images) and 20 μm for the magnified images. c, Heatmaps summarizing the frequency of melanoma cells stained positive for the MDAs TYR, MART-1 and gp100. The breadth of MDA expression was defined as the number of MDAs expressed per patient sample ranging from 0 (none) to 3 (all) as defined by values from ROC curves for each individual antigen. The breadth of T cell response (data from Fig. 1) is specified as the number of individual MDAs recognized, as indicated by the detection of IFN-γ+ CD8+ T cell responses, ranging from 0 (none) to 3 (all). d, Frequencies of melanoma cells showing positive staining for each of the MDAs TYR, MART-1 and gp100 in the analyzed tissue slides between R and NR. Dots represent individual patients, and lines indicate mean values. e, Correlation between the breadth of MDA expression and that of MDA- specific CD8+ T cell responses. Dots represent individual patients. Statistical analysis was performed using the Mann-Whitney test (d) and Spearman's correlation (e); *P < 0.05, **P < 0.01, ***P < 0.001.

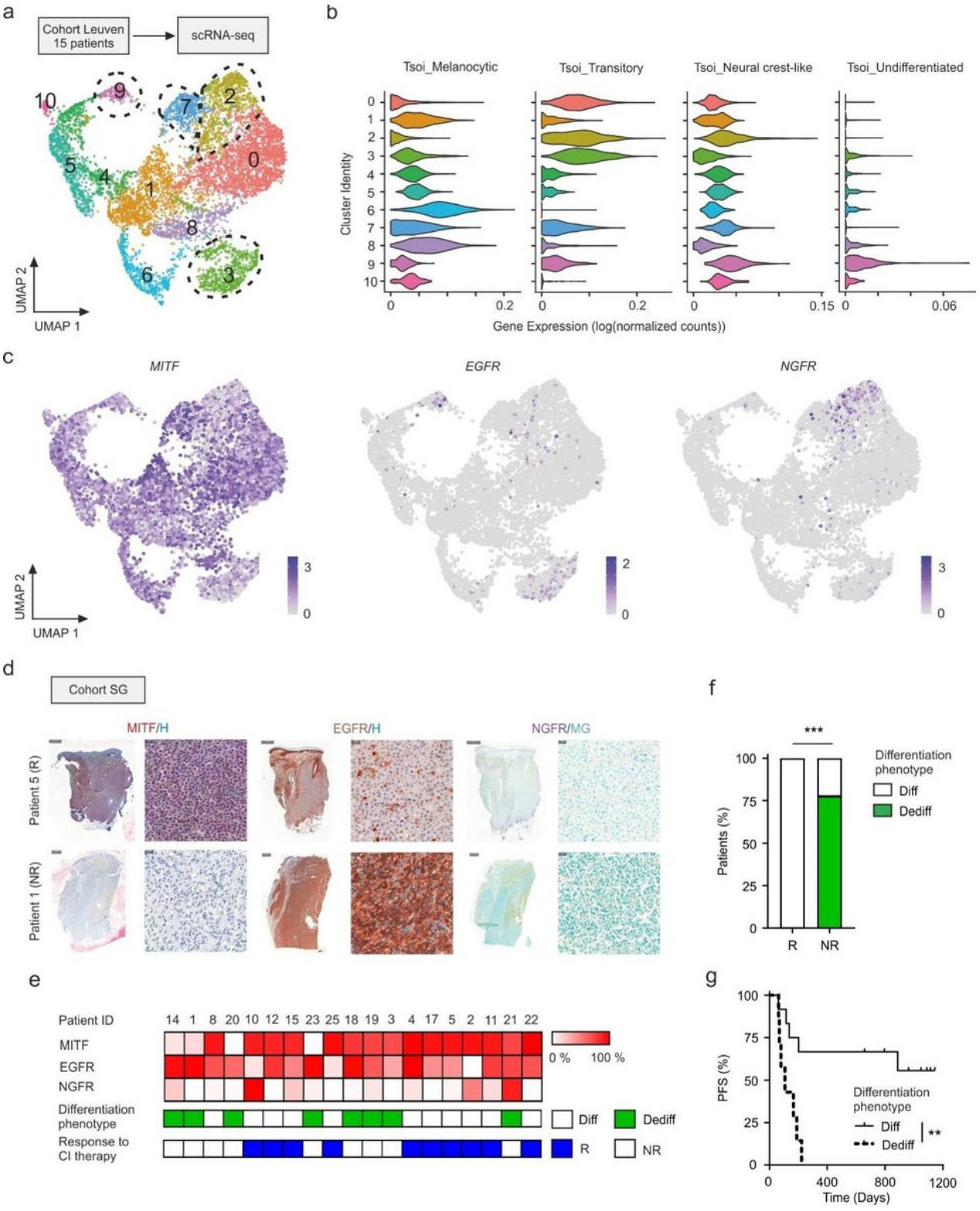

Figure 3

The dedifferentiated melanoma phenotype predicts patient outcome in response to checkpoint inhibitor therapy. a-c, We collected melanoma metastases from 15 stage III or stage IV treatment-naïve patients and performed single-cell RNA-seq analysis of tumor cells (Leuven cohort). a, UMAP plot displaying cluster assignment. Highlighted clusters harbor tumor cells with a dedifferentiated phenotype (cluster 2, 3, 7 and 9) whereas the other cluster exhibit a melanocytic and differentiated phenotype. b, Violin plots

based on the Tsoi et el. (2018) gene signatures for melanocytic, transitory, neural crest-like and undifferentiated melanoma phenotypes. c, UMAP plots showing the gene expression of MITF, EGFR and NGFR. d-g, In the SG cohort, the expression of MITF, EGFR and NGFR was assessed 290 in tumor biopsies obtained before initiation of checkpoint inhibitor therapy by quantitative IHC analysis. d, Representative images for the indicated antigens in patient 5 (R) and patient 1 (NR). The frequency oftumor cells expressing each of these antigens was assessed as outlined in Extended Data Figure 3. Hematoxylin (H) or Methyl Green (MG) staining to identify the cell nucleus. Scale bars are 500 and 2000 µm for the general images (top and bottom images) and 20 µm for the magnified images. e, Heatmaps summarizing the frequencies of melanoma cells showing positive staining for MITF, EGFR or NGFR using quantitative IHC analysis. The dedifferentiated melanoma phenotype (Dediff) was defined as MITFlow EGFRhigh or MITFlow NGFRhigh as based on threshold values from ROC curves for each individual protein. f, Proportions of patients in the 19 patients from the SG cohort with a dedifferentiated phenotype in the R and NR groups. g, Progression-free survival of patients with a dedifferentiated or differentiated melanoma phenotype. Statistical analysis was performed using the chi-square test (f) or the Mantel-Cox log-rank test (g); *P < 0.05, **P < 0.01, ***P < 0.001.

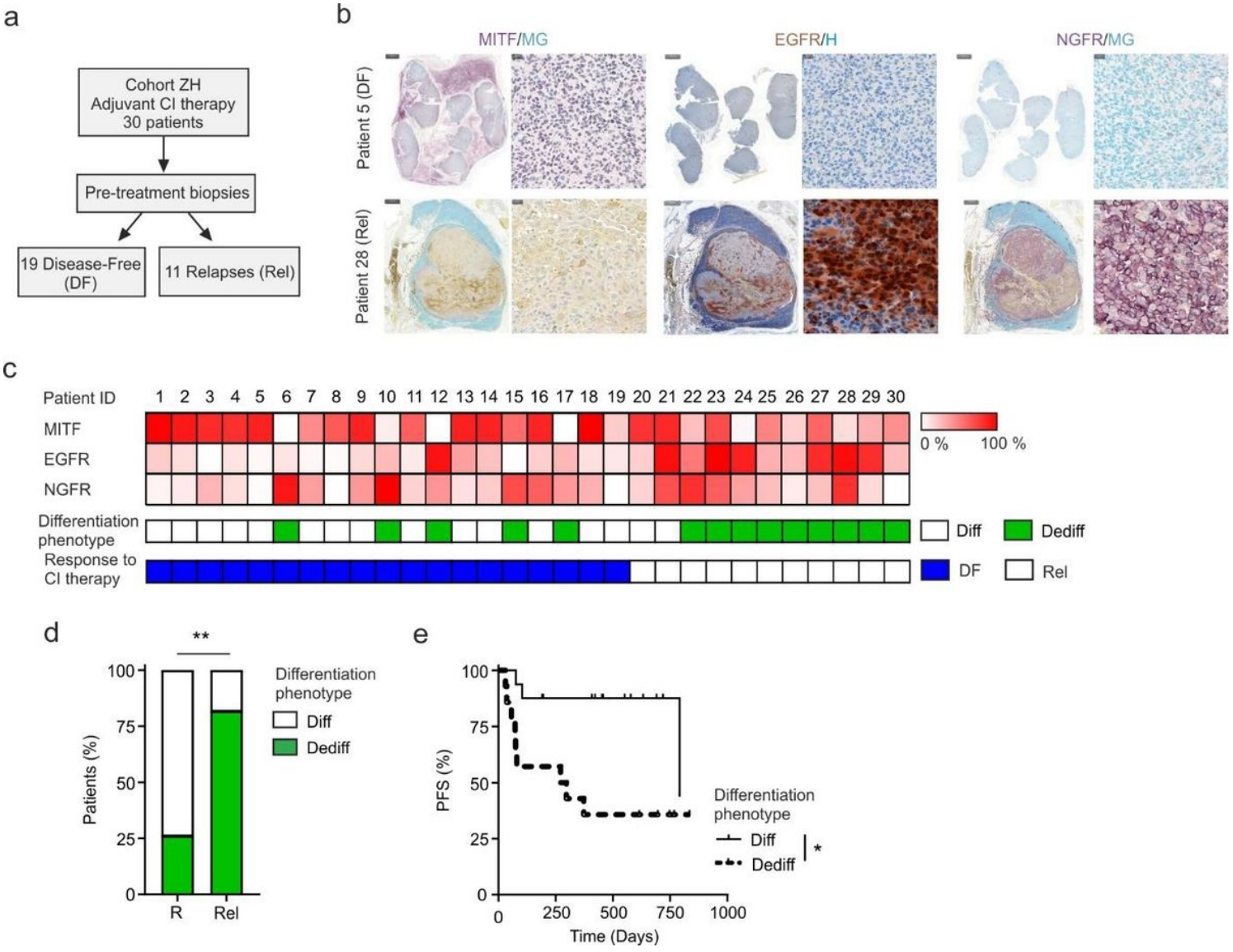

Figure 4

The dedifferentiated melanoma phenotype predicts patient outcome in response to adjuvant anti-PD-1 therapy. a, In the Zurich (ZH) adjuvant cohort, tumor biopsies were obtained before initiation of adjuvant anti-PD-1 treatment. Disease-Free patients (DF; R; n=19) and patients who experienced relapse (Rel; n=11) were determined at the first PET-CT scan within 3 months after start of therapy. b, Representative images showing the expression of MITF, EGFR and NGFR in patient 5 (DF) and patient 28 (Rel). The frequency of tumor cells expressing each of these antigens was assessed as outlined in Extended Data Figure 3. Hematoxylin (H) or Methyl Green (MG) staining to identify the cell nucleus. Scale bars are 1000 and 2000 μm for the general images (top and bottom images) and 20 μm for the magnified images. c, Heatmaps summarizing the frequency of tumor cells stained positive for MITF, EGFR and NGFR using quantitative IHC analysis. The dedifferentiated phenotype (Dediff) was defined as MITFlow EGFRhigh or MITFlow NGFRhigh and based on threshold values from ROC curves for each individual protein. d, Proportions of patients in the ZH adjuvant anti-PD-1 cohort with a dedifferentiated phenotype in the DF 318 and Rel groups. e, Progression-free survival of patients with a dedifferentiated or differentiated melanoma phenotype. Statistical analysis was performed using the chi-square test (d) or Mantel-Cox log-rank test (e); *P < 0.05, **P < 0.01, ***P < 0.001.